PURDUE UNIVERSITY
GRADUATE SCHOOL
Thesis/Dissertation Acceptance

This is to certify that the thesis/dissertation prepared

By _John Nathan Fitzpatrick_

Entitled
COUPLED THERMAL-FLUID ANALYSIS WITH FLOWPATH-CAVITY INTERACTION IN A GAS
TURBINE ENGINE

For the degree of ____Master of Science in Mechanical Engineering____

Is approved by the final examining committee:

Tamer Wasfy
_____
Chair

Razi Nalim
_____

Huidan (Whitney) Yu
_____

To the best of my knowledge and as understood by the student in the *Research Integrity and Copyright Disclaimer (Graduate School Form 20)*, this thesis/dissertation adheres to the provisions of Purdue University's "Policy on Integrity in Research" and the use of copyrighted material.

Approved by Major Professor(s): _Tamer Wasfy_

_____

Approved by: _Sohel Anwar_   12/02/2013
                 Head of the Graduate Program   Date

COUPLED THERMAL-FLUID ANALYSIS WITH FLOWPATH-CAVITY

INTERACTION IN A GAS TURBINE ENGINE

A Thesis

Submitted to the Faculty

of

Purdue University

by

John Nathan Fitzpatrick

In Partial Fulfillment of the

Requirements for the Degree

of

Master of Science in Mechanical Engineering

December 2013

Purdue University

Indianapolis, Indiana

ACKNOWLEDGMENTS

I would like to gratefully acknowledge my thesis advisor, Dr. Tamer Wasfy, for his assistance and guidance through much of my undergraduate and graduate course work in addition to the research and thesis work. Dr. Wasfy graciously shared his expertise and experience, especially in the field of computational fluid dynamics.

I would also like to thank my advisory committee members, Dr. Razi Nalim and Dr. Huidan (Whitney) Yu for their time and insight in the completion and evaluation of the thesis. I would also like to thank Ms. Valerie Lim Diemer for assisting me in formating my thesis.

I also wish to extend my very special thanks to my supervisor at Rolls-Royce Inc., Mr. Andrew White, who donated much of his busy schedule to giving advise and educating me on Rolls-Royce's proprietary software. I would also like to thank my boss at Rolls-Royce Inc., Mr. Paul Davis, who gracious gave me this opportunity of working on my thesis project for Rolls-Royce. I would like to acknowledge the other collaborators at Rolls-Royce who greatly aided in the completion of my thesis project. Mr. Jason Jacobs, Ms. Carol Nin, Mr. Dwayne Bevis, and Mr. Kevin Shanley contributed to my understanding of CFD, meshing, and aerodynamic theory. In addition Mr. Jason Jacobs aided me in leveraging his previous work on the HP compressor which was instrumental to the thesis. Mr. Antonio Guijarro aided in meshing difficult portions of the drive cone cavity. He also was a valuable resource in understanding the coupling procedure and setup. I would also like to thank Mr. Todd Simons for allowing me to use significant computational resources for the duration of the thesis.

And finally I would like to thank my friends and family who have aided and supported me throughout my life. I would especially like to express my sincerest thanks to my friends and classmates Garrett Yesmunt and Lukas Bearden who walked

along side me and supported and encouraged me throughout the duration of my college education.

TABLE OF CONTENTS

LIST OF TABLES

LIST OF FIGURES

LIST OF SYMBOLS

m mass

v velocity

κ von Kàrmàn constant ($= 0.418$)

k_P turbulent kinetic energy at the first near-wall node P

E empirical constant ($= 9.793$)

U_p mean velocity at the near-wall node P

U^* nondimensional near-wall velocity

y_P distance from point P to wall

y^* nondimensional near-wall distance

y_T^* nondimensional thermal sublayer thickness

μ fluid dynamic viscosity

ρ density of fluid

$\dot{q}$ wall heat flux

T_p fluid temperature at the first near-wall node P

T_w wall temperature

Pr Prandtl number ($\mu c_p / k_f$)

Pr_t turbulent Prandtl number ($= 0.85$)

A Van Driest constant ($= 26$)

U_c mean velocity magnitude at $y^* = y_T^*$

LIST OF ABBREVIATIONS

CFD   computational fluid dynamics

FEA   finite element analysis

HTC   heat transfer coefficient

MTO   max take off

LP   low pressure

IP   intermediate pressure

HP   high pressure

DCC   drive cone cavity

OGV   outlet guide vein

ABSTRACT

Fitzpatrick, John Nathan. M.S.M.E., Purdue University, December 2013. Coupled Thermal-fluid Analysis with Flowpath-Cavity Interaction in a Gas Turbine Engine. Major Professor: Tamer Wasfy.

This study seeks to improve the understanding of inlet conditions of a large rotor-stator cavity in a turbofan engine, often referred to as the drive cone cavity (DCC). The inlet flow is better understood through a higher fidelity computational fluid dynamics (CFD) modeling of the inlet to the cavity, and a coupled finite element (FE) thermal to CFD fluid analysis of the cavity in order to accurately predict engine component temperatures. Accurately predicting temperature distribution in the cavity is important because temperatures directly affect the material properties including Young's modulus, yield strength, fatigue strength, creep properties. All of these properties directly affect the life of critical engine components. In addition, temperatures cause thermal expansion which changes clearances and in turn affects engine efficiency. The DCC is fed from the last stage of the high pressure compressor. One of its primary functions is to purge the air over the rotor wall to prevent it from overheating. Aero-thermal conditions within the DCC cavity are particularly challenging to predict due to the complex air flow and high heat transfer in the rotating component. Thus, in order to accurately predict metal temperatures a two-way coupled CFD-FE analysis is needed. Historically, when the cavity airflow is modeled for engine design purposes, the inlet condition has been over-simplified for the CFD analysis which impacts the results, particularly in the region around the compressor disc rim. The inlet is typically simplified by circumferentially averaging the velocity field at the inlet to the cavity which removes the effect of pressure wakes from the upstream rotor blades. The way in which these non-axisymmetric flow characteristics affect metal temperatures is not well understood. In addition, a constant air temperature scaled from a

previous analysis is used as the simplified cavity inlet air temperature. Therefore, the objectives of this study are: (a) model the DCC cavity with a more physically representative inlet condition while coupling the solid thermal analysis and compressible air flow analysis that includes the fluid velocity, pressure, and temperature fields; (b) run a coupled analysis whose boundary conditions come from computational models, rather than thermocouple data; (c) validate the model using available experimental data; and (d) based on the validation, determine if the model can be used to predict air inlet and metal temperatures for new engine geometries.

Verification with experimental results showed that the coupled analysis with the 3D no-bolt CFD model with predictive boundary conditions, over-predicted the HP6 offtake temperature by 16k. The maximum error was an over-prediction of 50k while the average error was 17k. The predictive model with 3D bolts also predicted cavity temperatures with an average error of 17k. For the two CFD models with predicted boundary conditions, the case without bolts performed better than the case with bolts. This is due to the flow errors caused by placing stationary bolts in a rotating reference frame. Therefore it is recommended that this type of analysis only be attempted for drive cone cavities with no bolts or shielded bolts.

1. INTRODUCTION

1.1 Motivation

In the aero-engine market, engine manufacturers must meet both customer and regulatory demands while maintaining a high enough profit margin to stay in business. Customers are always eager to buy engines that weigh less, are more efficient, last longer, and produce less noise and pollution. At the same time, an engine must be proven structurally sound and airworthy for the duration of its expected life. Engineers must also reduce development costs by making predictions in shorter time-frames, and reducing the number of physical experiments during design iterations. To this end, the primary aim of this study is to model the inlet airflow conditions of the rotor-stator cavity fed from the high pressure compressor in a typical 3-shaft engine, Figure 1.1. The inlet condition of rotor stator cavities is typically modeled as an axisymetric simplification of the airflow. The improved understanding of the inlet conditions will be used to run a coupled solid FEA to CFD analysis to accurately predict air inlet and metal temperatures in the cavity.

Accurately predicting metal temperatures is a key factor in the design process because temperatures directly affect the material properties including Young's modulus, yield strength, fatigue strength, creep properties, and melting point. All of these properties directly affect the life of critical engine components. After component temperatures are predicted they are given as inputs to stress engineers. Stress engineers use temperatures combined with other inputs such as mechanical loads to calculate stresses in areas of the engine which are of interest. These stress and temperature predictions are used to determine the expected life of components which will ultimately determine if a part is over, adequately, or under-designed. Under-designed parts can shorten the life of the engine and even result in catastrophic failures, while
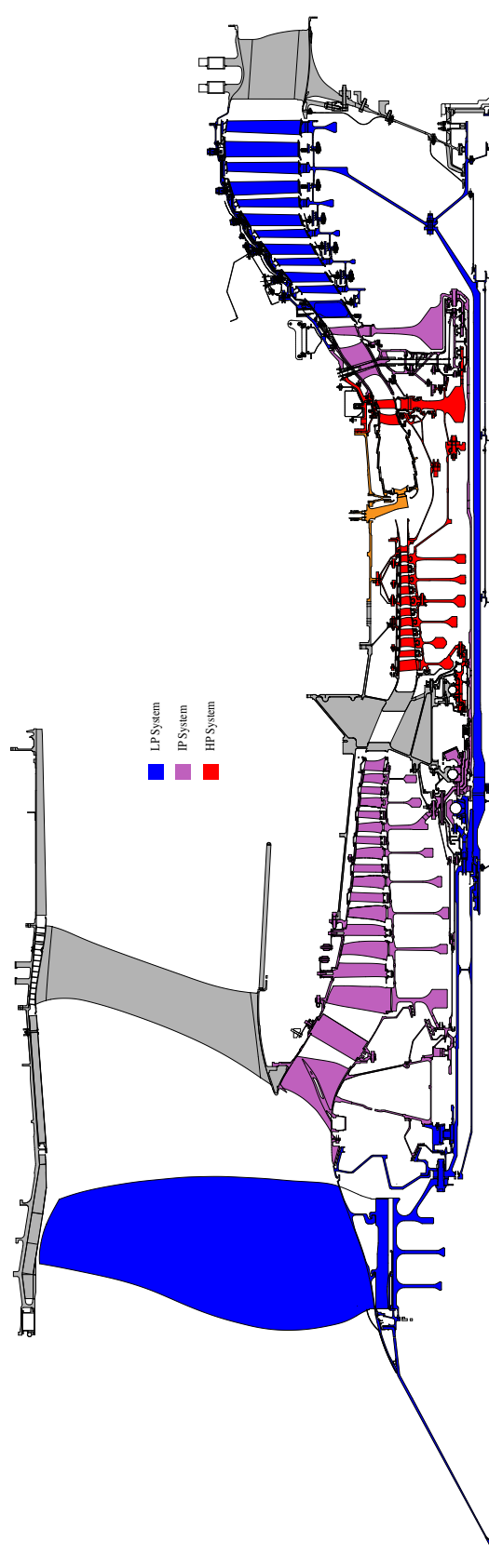
Figure 1.1. Typical geometry for a three-shaft gas turbine engine. The three shafts rotate at different speeds as designated by the colors in the key. Gray portions of the graph are non rotating components.

over-designed parts can increase the weight of the engine thereby decreasing its range. Therefore, the predictive accuracy of stress and life models depends on the accurate prediction of metal temperatures.

Accurate metal temperatures are also needed for predicting rotor tip clearances. As the rotor blades heat up, thermal expansion causes the blades to grow and the tips to approach the outer wall of the engine. The closer the blades can get to the outer wall without contacting the wall, the more efficient the engine will be.

The present study is concerned with predicting metal temperatures at the final stages of the HP compressor of a Rolls-Royce Inc. gas turbine engine, specifically the drive cone cavity, Figure 1.2. The drive cone cavity, also known as the HP6 air system, bleeds air from the 6th stage of the HP compressor. This fraction of airflow taken from the main gas path serves three purposes.

1. The air is used to purge the drive cone cavity. The drive cone is one of the hottest components in the engine. If the air in the cavity had no through-flow then the windage (viscous friction heating) generated by the drive cone would cause it to overheat and fail.

2. Air leaks through the labyrinth seals on the aft end of the cavity and provides positive pressure at the HP turbine stage. This positive pressure prevents hot gas from the combustor entering the turbine rim rotor-stator cavity and melting the components.

3. Some air from the HP6 cavity is used to cool the HP turbine.

The engine will run more efficiently if the air is compressed to a higher pressure. Since pressure is directly proportional to temperature by the ideal gas law, components in the final compressor stages are often operating near the limit of the material's abilities. At the MTO condition, an increase in temperature of only 10 degrees is estimated to cut the life of the drive cone in half. Such a small margin of error necessitates a knowledge of metal temperatures with a great degree of accuracy. The
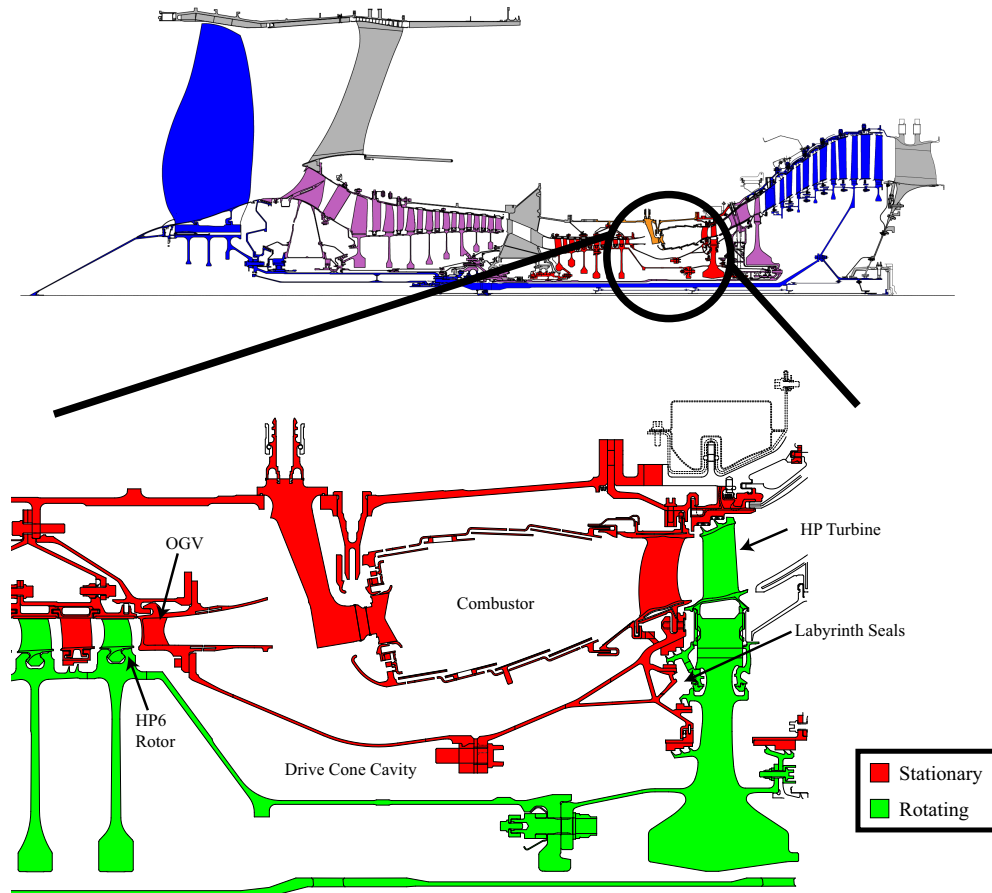
Figure 1.2. The Drive Cone Cavity

analysis tool used at Rolls-Royce Inc. for predicting metal temperatures is an in-house finite element code called sc03, see Section 2.7. This code solves the transient heat conduction equation and uses a series of 1-D boundary conditions to represent airflow over the metal surfaces. Standard correlations for HTC, windage, etc. in the boundary conditions scale with rotor speed. This means that an entire test flight can be simulated as a transient analysis, and metal temperatures can be calculated at each stage of an engine cycle. One example of a commonly used boundary condition is the *stream* function. The stream boundary condition represents a stream of air flowing over the metal. Energy is exchanged between the stream and the boundary walls which is then carried along the path of the airflow. The heat transfer coefficient

used to determine the heat flux between the walls and the air is often the free disk correlation [1] which is a function of rotor speed. The advantage of this software is that it can run an entire test flight which is an approximately 1 hour transient analysis in 5 to 6 hours on a standard workstation. The ability to predict metal temperatures throughout the engine for all flight conditions such as idle, cruise, and max-take-off, in only 5 to 6 hours is convenient for analysts since a simulation can be done in one work day.

The typical design cycle in a modern turbine engine usually begins with a previous design. The previously designed engine, preferably one with a similar geometry, has already been tested and approved for commercial use and is often already in production. The new design is thus an incremental change in the reference design, expected to improve efficiency, durability, and/or range of flight. The conventional process for predicting metal temperatures for a new engine begins by using the analysis from a similar previous engine. The previous analysis did not necessarily predict metal temperatures well, but test data from that engine exists which is used to improve that analysis through a process called *matching*. Matching is a tedious procedure which can take even an experienced engineer several months to complete. In short, the various inputs to boundary conditions throughout the engine are multiplied by correction factors which make the metal temperatures more closely resemble thermocouple test data. The process involves a long series of trial and error and *tweaking* the correction factors until metal temperatures are matched.

The problem with this approach is that if the geometry for a new design is a significant departure from the reference design then sc03 cannot predict the new metal temperatures with a great deal of confidence. Experienced engineers can do their best to predict how the change in geometry will affect the boundary conditions, but there is a great deal of subjectivity in the matching process. In addition, just because a matching exercise yields analytical wall temperatures that are close to measured temperatures does not mean that the physics are being accurately captured in the analysis.

The lack of confidence in the analysis for new engines necessitates a more objective approach. CFD is a tool that is used extensively to solve fluid flow through complex geometry. There are a number of ways in which CFD could be used to reduce the uncertainty in an engine thermal analysis and provide results in a more timely manner. Some of these are listed below:

1. For engine designs with significantly new geometry, flow velocity profiles and mass flow rates calculated from the CFD solution could be used to set boundary conditions in sc03.

2. Heat transfer coefficients are the parameter that is most often "tweaked" in matching exercises. Heat flux and heat transfer coefficients calculated from CFD could be used to determine which correlations best approximate the CFD results and which scaling factors should be used.

3. CFD analysis and FE analysis could be solved simultaneously within the same code. This is known as solving the conjugate problem.

4. Conventional sc03 boundary conditions could be replaced by boundary conditions that iteratively pass heat flux and wall temperatures back and fourth between sc03 and the CFD analysis. Thus the solid and fluid analyses would be coupled.

All 4 methods have been implemented for a number of applications at Rolls-Royce Inc. Because the goal of the present study is to predict metal temperatures in the drive cone cavity with as much fidelity and as little computational cost as possible (see Section 1.2.2), a coupled solid FEA-CFD analysis (method 4) is the approach being implemented.

Although coupled analyses of rotor-stator cavities have been performed previously, see [9], all such known simulations have oversimplified inlet boundary conditions. The present study seeks to improve the analysis through a higher fidelity inlet. Specifically, the CFD analysis consists of a 3D sector mesh and the main gaspath includes rotor

blades upstream of the cavity as well as stator blades downstream. Because it is necessary for the air surrounding the rotor to be modeled in the rotating reference frame, it is common practice to put a mixing plane upstream of the cavity so that the air in the cavity the stator air in the absolute reference frame. However, the downside of using a mixing plane is that it circumferentially averages the flow at the exit plane of the rotor blades. Thus all circumferential variation in the flow is lost inside the cavity. To avoid this simplification, the mixing plane will be placed downstream of the cavity inlet. In order to compensate for the change in reference frames, the boundary conditions of rotor and stator walls in the cavity are adjusted accordingly.

1.2 Previous Work

The conventional method for solving metal temperatures in a gas turbine engine has been using software which only solves the heat conduction equation. The boundary conditions on the metal surfaces have been defined by empirical correlations which represent the physics of the solid-fluid interaction. This process is outlined by Monico and Chew [2]. However standard correlations do not often accurately represent the physics involved at the fluid-solid boundary for complex aero-engine geometry. Therefore, computational fluid dynamics has been used to improve upon this conventional method in two fundamental ways:

1. CFD has been used to examine specific parameters such as windage and heat transfer coefficients at the fluid boundaries. The knowledge about these parameters assists engineers in choosing proper correlations and correction factors on conventional metal boundary conditions.

2. Fluid flow equations in CFD and heat conduction equations in a finite element solver are solved simultaneously or iteratively until the boundary wall temperatures converge. Thus the solid and fluid analyses are coupled.

1.2.1   CFD Assisted Boundary Conditions

Lewis and Provins [3] have used CFD in the drive cone cavity to develop a windage correlation for engines with different mass flows, angular velocities, and geometry. This simple correlation was used to calculate the windage in boundary conditions for an uncoupled finite element solver. This method does not require CFD to be run for a new engine design, so turn-around time for thermal results is much shorter than for a coupled analysis. Although using this correlation in a stand-alone finite element solver is very computationally efficient, it was found that after comparison with thermocouple data the suggested approach does not yield metal temperature results that are as accurate as a coupled analysis.

CFD analysis has previously been used to aid in the determination of wall temperatures by comparing standard correlations of convective heat transfer coefficients to HTC's obtained by a CFD code for the particular geometry in question. Thus an appropriate correlation and "correction factor" would be chosen to match the HTC's in the heat conduction analysis boundary conditions to the HTC's obtained by CFD. A study by Evans et al [4] concluded that Fluent, the widely used commercial CFD code, could predict heat transfer coefficients which accurately matched experimental data from a test rig. The predicted heat transfer coefficients were then compared to standard correlations to investigate which one gave the best fit. This study suggests that CFD is a reliable tool for accurately determining heat transfer coefficients for a new or unknown engine geometry.

A numerical investigation of drive cone cavity flow was conducted by Verdicchio et al. [5]. This study compares CFD results from a 2D axisymetric model, a 3D axisymetric model without tip clearance, and a 3D axisymetric model with tip clearance to experimental results from an engine test rig. Both 3D models include the main gas path with rotor blades, but the one with tip clearance accurately models the actual gap between the tip of the rotor blade and the casing. The results show that the flow in the cavity was sensitive to the rotor tip gap. The 3D case which accurately modeled

the tip gap produced axial and tangential (swirl) flows which matched experimental data much more closely than the case that did not. Thus it can be concluded that correctly modeling the rotor features are important in determining the inlet conditions to the drive cone cavity. It was also found that the 2D axisymetric case was sensitive to the initial tangential velocity specified at the inlet. The 2D case produced results similar to the 3D (with tip clearance) case, but only when a suitable inlet swirl velocity was chosen.

A study by Dixon et al. [6] compared CFD results from a 3D sector of the drive cone cavity to experimental results from a test rig of the same cavity. The CFD model included the effects of ingestion from the main annulus with a 3D rotor. A $k - \varepsilon$ turbulence model was used with standard wall functions. The CFD models showed "good agreement" with the axial and tangential (swirl) velocity measured from the test rig and "reasonably good agreement" when comparing heat flux. In addition, the predicted HTC's from the CFD were used to identify a good correlation, which was used in the boundary conditions of SC03. This study provides validation for CFD as a predictive tool in determining airflow and heat transfer in a drive cone cavity.

Dixon [7] also used CFD to determine heat transfer coefficients for the purpose of determining wall temperatures for new engine geometry. Dixon would first run a steady state CFD analysis with adiabatic walls at the engine condition of interest, then run two more CFD analyses at wall temperatures approximately 50K above and below the adiabatic wall temperatures, and extract the wall heat fluxes for each condition. The heat transfer coefficients were then calculated by the following equation:

$$htc = \frac{Q_1 - Q_2}{T_1 - T_2} \tag{1.1}$$

which is derived from Newton's law of cooling:

$$Q_1 = h\left(T_1 - T_f\right)$$

and

$$Q_2 = h\left(T_2 - T_f\right) \tag{1.2}$$

where T_f is fluid temperature, and T_1 and T_2 are wall temperatures. Dixon uses this entire procedure iteratively between CFD and the finite element code (SC03) to calculate the "correct" wall temperatures for a stabilized condition. This, in effect, is a manual coupling of CFD and FEA codes.

1.2.2 Automated CFD/FEA Coupling

There exist two techniques for automating the process of passing heat flux from the CFD solution to the FEA solution, and wall temperatures from the FEA solution back to the CFD:

1. Solve the fluid flow equations and the heat conduction equations in the same solver. This is known as solving the 'conjugate' problem. The advantage of solving both sets of equations in the same code is that the equations can be solved simultaneously rather than iteratively, which can speed up overall solve time.

2. Solve the heat conduction equations in one code and the fluid flow equations in another code. This is known as a 'coupled' solution. For this problem, heat flux and wall temperature boundary conditions are passed back and forth iteratively between the two codes until the wall temperature boundary conditions of both codes converge. The advantage of solving the coupled problem in two codes is that if the FEA solver had specialized boundary conditions, solid metal temperatures can be solved in regions where CFD is either not required, or too computationally expensive to be practical.

One of the first attempts at solving metal heat conduction equations and fluid flow equations simultaneously for the HP drive cone cavity was by performed by Verdicchio and Lewis [8] in 1996. The cavity was 2D and therefore did not include the 3D effects of the rotor or stator. Fluent was used for this analysis to solve the 2D conjugate problem, meaning the CFD and thermal conduction equations were solved in the same code.

In the present study, the heat conduction solver being used is the in-house code, SC03, which utilizes specialized boundary conditions such as streams, ducts, and voids which simulate fluid flow at metal boundaries without the computational expense involved in solving fluid flow equations. Such boundary conditions are not available in a conjugate solver such as ANSYS Fluent which is why the present study utilizes the 'coupled' technique.

The coupling of CFD with Rolls-Royce's in-house code SC03 was first introduced by Verdicchio in his 2001 PhD thesis [9]. In his thesis, Verdicchio performs a coupled analysis for two drive cone cavities from different engines. Both were 2D axisymetric with ingestion from the main gaspath. He also performed a turbulence model sensitivity study with a 2-layer model and a standard $k - \varepsilon$ model. He concluded that the boundary heat flux in the $k - \varepsilon$ model matched the 2-layer model sufficiently well and with far less computational cost. Therefore, the decision was made to use the $k - \varepsilon$ turbulence model for all the analyses in the study. For this reason the $k - \varepsilon$ model is used for all of the analyses in the present study as well. To perform the coupling, Verdicchio developed an ANSI C program which automated the process of writing out wall temperatures from SC03 as Fluent temperature profiles, running Fluent, writing out heat flux profiles and reading them into SC03, and repeating until the wall temperatures converged.

Mirzamoghadam and Xiao [10], performed a CFD/FEA coupled analysis for a rotor-stator rim sealing cavity. As in the present study, Mirzamoghadam and Xiao used Fluent to perform the CFD analysis and Rolls-Royce's proprietary finite element code, SC03, for the heat conduction analysis. Both the CFD and finite element models

were 2D axisymetric, but very little is said about how the actual coupling process is achieved.

Barnes et al. [11] performed a transient coupling analysis of four test cases including a HP compressor drive cone cavity. The CFD domain for the drive cone cavity was a 2D axisymetric model with a truncated gaspath. Once all CFD equations had converged, eg. velocity components, turbulence, and energy, only the energy equation was re-solved during the actual coupling procedure. This is an approximation following from the observation that the flow field changes very little at a particular engine condition. Therefore, since the only thing of interest from the CFD analysis is the heat flux at the boundaries, only the energy equation was solved during the iterations between Fluent and SC03.

The coupling process has been applied to other regions of the engine as well. Lewis et al. [12] performed a transient coupling analysis for an IP turbine disk cavity. The cavity CFD model was a 3D mesh with asymmetric inlet holes. The results of the analysis were compared only to more conventional baseline models, not to test data. Therefore, the true accuracy of the method was not determined. A similar cavity was coupled by Barnes et al. [13]. A 3D domain was used to model an HP turbine pre-swirl cavity, which was compared to a 2D axisymetric model of the same cavity as well as a more conventional standalone finite element modeling approach. However, none of the models were compared to test data so it is difficult to judge the accuracy of any of these methods.

Dixon et al. [14] performed a coupling analysis of a turbine hub cavity with ingestion from the main annulus. The CFD model was a 3D sector which included a rotor blade and guide vane in the gaspath which was coupled with a 2D axisymetric finite element model. Both transient and steady state CFD analyses were run and showed good agreement with test data.

In addition to their work investigating the flow in a compressor drive cone cavity, Dixon et al. [6] performed a transient coupled analysis of a turbine disk cavity. The coupled analysis largely under-predicted metal temperatures in the cavity. One pos-

sible explanation is that the CFD mesh was 2D and did not model features such as bolts which tend to increase windage in cavities.

Barnes et al. [15] take the coupling process a step further and perform a fluid-thermo-mechanical coupling analysis. Heat flux and wall temperatures were passed between the CFD and FEA analyses using the process already described, with one additional iterative loop. At each time step the CFD mesh was adapted to reflect the change in geometry predicted by solving the structural equations in the finite element code. The mesh is adapted using the spring analogy. The spring analogy works by imagining the CFD mesh as a structural net of springs where the strength of each spring is inversely proportional to the length of the edge. Thus, as the CFD boundary walls are displaced, the cells of the mesh displace without intersecting each-other. Barnes et al. applied this coupling process to an interstage seal cavity where flow through the labyrinth seal is greatly affected by the seal clearance. The fluid domain was represented by a 2D CFD mesh with gaspath interaction, and the finite element model was also 2D. In the present study the thermo-mechanical displacement of the solid model is considered to have a negligible effect on fluid flow. Therefore, the structural equations are not solved in the finite element model, nor is there any fluid mesh adaptation.

A transient coupling analysis involving five separate engine cavities was performed by Hills et al. [16]. All five CFD domains were 2D, and the finite element model was 2D as well. The five domains modeled were the drive cone cavity, upper preswirl, lower preswirl, bore, and rear IP turbine cavities. All cavities were run in Rolls-Royce's in-house CFD code HYDRA. The results given by the study show that temperatures were under-predicted by the coupling analysis. Once again the authors speculate that this may be due to the 2D simplification of the fluid domains. The addition of 3D features which create windage heating might make the coupled analysis more accurate.

1.3   Objectives

Historically, when the cavity airflow is modeled for engine design purposes, the inlet condition has been over-simplified for the CFD analysis which impacts the results, particularly in the region around the compressor disc rim. The inlet is typically simplified by circumferentially averaging the velocity field at the inlet to the cavity which removes the effect of pressure wakes from the upstream rotor blades. The way in which these non-axisymetric flow characteristics affect metal temperatures is not well understood. In addition, a constant inlet air temperature is scaled to match an air temperature read from a thermocouple from a previous design, see Section 3.1.3. However, if the boundary conditions and/or geometry change significantly between engine designs, this matched scaling factor may no longer be valid. Therefore, the objectives of this study are:

1. Model the DCC cavity with a more physically representative inlet condition while coupling the solid thermal analysis and compressible air flow analysis that includes the fluid velocity, pressure, and temperature fields. This specifically means attaching a portion of the main annulus that includes the HP6 rotor and OGV, Figure 1.2. It also includes adding the 3D flange bolts and OGV nuts to the CFD mesh.

2. Run a coupled analysis whose boundary conditions come only from computational models, rather than thermocouple data. The performance group of Rolls-Royce Inc. predicts the pressures and temperatures on both ends of the high pressure compressor (P_{26} and T_{26} at the compressor inlet, and P_{30} and T_{30} at the compressor outlet). These predictions are then calibrated using experimental data from a test rig. For a new engine design only these predictions, secondary airflow predictions, and the geometry are available. One of the goals of this study is to use only these inputs, rather than thermocouple data from a previous analysis, to predict metal temperatures in the DCC.

3. Validate the model using available experimental data by comparing the predicted metal temperatures at reference locations to thermocouple data at those locations.

4. Based on the validation, determine if the model can be used to predict metal temperatures for new engine geometries.

2. GOVERNING EQUATIONS

2.1 Basic Fluid Flow

The computational fluid dynamics (CFD) analysis in this research was performed with ANSYS FLUENT version 6.3, hereafter referred to as "FLUENT." FLUENT is a commercial CFD code, widely used in industry and academia. Only the fundamental governing equations which are relevant to this thesis are presented. For more information about FLUENT, the reader may refer to FLUENT's user guide [17] and theory manuals [18].

The Navier Stokes system of equations for 3D and 2D axisymetric flow are presented below.

For 3D Flow:

(In Einstein Summation Notation) The conservation of mass is given as:

$$\frac{\partial \rho}{\partial t} + \frac{\partial}{\partial x_i}\left(\rho u_i\right) = 0 \tag{2.1}$$

where ρ is density, u = velocity component, x = spacial direction

The conservation of momentum is given as:

$$\frac{\partial}{\partial t}\left(\rho u_i\right) + \frac{\partial}{\partial x_j}\left(\rho u_i u_j\right) = \frac{\partial p}{\partial x_i} + \frac{\partial}{\partial x_j}\left(\tau_{ij}\right) \tag{2.2}$$

The conservation of energy is given as:

$$\frac{\partial}{\partial t}\left(\rho h - p + \frac{\rho u_i^2}{2}\right) + \frac{\partial}{\partial x_i}\left[u_i \rho \left(h + \frac{u_i^2}{2}\right)\right] = \frac{\partial}{\partial x_i}\left[k_{\text{eff}}\frac{\partial T}{\partial x_i} + u_j \left(\tau_{ij}\right)_{\text{eff}}\right] \tag{2.3}$$

where μ is viscosity, and the stress tensor τ_{ij} is given by:

$$\tau_{ij} = \left[\mu \left(\frac{\partial u_i}{\partial x_j} + \frac{\partial u_j}{\partial x_i} \right) \right] - \frac{2}{3} \mu \frac{\partial u_k}{\partial x_k} \delta_{ij} \tag{2.4}$$

where δ_{ij} is the Kronecker delta, k_{eff} is the effective thermal conductivity defined as:

$$k_{\text{eff}} = k_{thermal} + k_t \tag{2.5}$$

where, $k_{thermal}$, and k_t are the thermal conductivity, and turbulent thermal conductivity respectively.

$(\tau_{ij})_{\text{eff}}$ is the deviatoric stress tensor defined as τ_{ij} in equation, (2.4), with μ replaced with μ_{eff}, defined as:

$$\mu_{\text{eff}} = \mu + \mu_t \tag{2.6}$$

where μ_t is the turbulent viscosity.

and h is enthalpy, defined as:

$$h = \int_{T_{\text{ref}}}^{T} C_p dT \tag{2.7}$$

where C_p is specific heat at constant pressure, and T_{ref} is a given reference temperature.

For 2D axisymetric analyses: The conservation of mass equation:

$$\frac{\partial \rho}{\partial t} + \frac{\partial}{\partial x} \left(\rho u \right) + \frac{\partial}{\partial r} \left(\rho v \right) + \frac{\rho v}{r} = 0 \tag{2.8}$$

The radial, axial, and tangential momentum equations:

$$\begin{aligned}
\frac{\partial}{\partial t} \left(\rho v_x \right) + \frac{1}{r} \frac{\partial}{\partial x} \left(r \rho v_x v_x \right) + \frac{1}{r} \frac{\partial}{\partial r} \left(r \rho v_r v_x \right) &= -\frac{\partial p}{\partial x} \\
&\quad + \frac{1}{r} \frac{\partial}{\partial x} \left[r \mu \left(2 \frac{\partial v_x}{\partial x} - \frac{2}{3} \left(\nabla \cdot \vec{v} \right) \right) \right] \\
&\quad + \frac{1}{r} \frac{\partial}{\partial r} \left[r \mu \left(\frac{\partial v_x}{\partial r} + \frac{\partial v_r}{\partial x} \right) \right] + F_x
\end{aligned} \tag{2.9}$$

$$\frac{\partial}{\partial t}(\rho v_r) + \frac{1}{r}\frac{\partial}{\partial x}(r\rho v_x v_r) + \frac{1}{r}\frac{\partial}{\partial r}(r\rho v_r v_r) = -\frac{\partial p}{\partial r}$$
$$+ \frac{1}{r}\frac{\partial}{\partial x}\left[r\mu\left(2\frac{\partial v_r}{\partial r} - \frac{2}{3}(\nabla \cdot \vec{v})\right)\right]$$
$$+ \frac{1}{r}\frac{\partial}{\partial x}\left[r\mu\left(\frac{\partial v_r}{\partial x} + \frac{\partial v_x}{\partial r}\right)\right]$$
$$- 2\mu\frac{v_r}{r^2} + \frac{2}{3}\frac{\mu}{r}(\nabla \cdot \vec{v}) + \rho\frac{v_z^2}{r} + F_x$$

$$(2.10)$$

$$\frac{\partial}{\partial t}(\rho w) + \frac{1}{r}\frac{\partial}{\partial x}(r\rho uw) + \frac{1}{r}\frac{\partial}{\partial r}(r\rho vw) = \frac{1}{r}\frac{\partial}{\partial x}\left[r\mu\frac{\partial w}{\partial x}\right]$$
$$+ \frac{1}{r^2}\frac{\partial}{\partial r}\left[r^3\mu\frac{\partial}{\partial r}\left(\frac{w}{r}\right)\right] - \rho\frac{vw}{r}$$

$$(2.11)$$

where

$$\nabla \cdot \vec{v} = \frac{\partial u}{\partial x} + \frac{\partial v}{\partial r} + \frac{v}{r} \tag{2.12}$$

The conservation of energy equation:

$$\frac{\partial}{\partial t}\left(\rho h - p + \frac{\rho \bar{v}^2}{2}\right) +$$
$$\frac{1}{r}\frac{\partial}{\partial x}\left(r\rho u\left[h + \frac{u^2}{2}\right]\right) +$$
$$\frac{1}{r}\frac{\partial}{\partial r}\left(r\rho u\left[h + \frac{v^2}{2}\right]\right) = \frac{1}{r}\frac{\partial}{\partial x}\left[rk_{\text{eff}}\frac{\partial T}{\partial x} + u(\tau_{xx})_{\text{eff}} + v(\tau_{xr})_{\text{eff}} + w(\tau_{xw})_{\text{eff}}\right]$$
$$+ \frac{1}{r}\frac{\partial}{\partial r}\left[rk_{\text{eff}}\frac{\partial T}{\partial r} + u(\tau_{rx})_{\text{eff}} + v(\tau_{rr})_{\text{eff}} + w(\tau_{rw})_{\text{eff}}\right]$$

$$(2.13)$$

x is the axial coordinate, r is the radial coordinate, u is the axial velocity, v is the radial velocity, and w is the swirl velocity.

Because the flow through the engine compressor is characterized by high Mach numbers, compressibility effects are not negligible. For compressible flows density is solved from the ideal gas law as follows:

$$\rho = \frac{p_{op} + p}{\frac{R}{M_w}T} \tag{2.14}$$

where p_{op} is the user defined operating pressure, and p is static pressure. Together, $p_{op} + p$ is absolute pressure. R is the universal gas constant, M_w is the molecular weight, and T is temperature computed from the energy equation.

2.2 Turbulence

The standard $k - \varepsilon$ model is a 2 equation turbulence model developed by Launder and Spalding [19]. In his PhD thesis [9], J.A. Verdicchio used the standard $k - \varepsilon$ turbulence model for all of the CFD analyses. It was chosen because of robustness and wide acceptance in industrial applications, and it gave comparable results to more computationally expensive turbulence schemes. The turbulent kinetic energy, (k), and the dissipation rate, (ε), are obtained from the following transport equations:

$$\frac{\partial}{\partial t}(\rho k) + \frac{\partial}{\partial x_i}(\rho k u_i) = \frac{\partial}{\partial x_i}[\tau_{ij}u_j] + \frac{\partial}{\partial x_i}\left[\left(\mu + \frac{\mu_t}{\sigma_k}\right)\frac{\partial k}{\partial x_i}\right] - \rho\varepsilon \tag{2.15}$$

$$\frac{\partial}{\partial t}(\rho\varepsilon) + \frac{\partial}{\partial x_i}(\rho\varepsilon u_i) = \frac{\partial}{\partial x_i}\left[\left(\mu + \frac{\mu_t}{\sigma_\varepsilon}\right)\frac{\partial\varepsilon}{\partial x_i}\right] + C_{\varepsilon 1}\frac{\partial}{\partial x_i}(\tau_{ij}u_j) - C_{\varepsilon 2}\rho\frac{\varepsilon^2}{k} \tag{2.16}$$

where the turbulent viscosity μ_t is defined as:

$$\mu_t = \rho c_\mu \frac{k^2}{\varepsilon} \tag{2.17}$$

and where $c_\mu, c_{\varepsilon 1}, c_{\varepsilon 2}, \sigma_k$, and σ_ε are model constants.

$c_\mu = 0.09$

$c_{\varepsilon 1} = 1.44$

$c_{\varepsilon 2} = 1.92$

$\sigma_k = 1.0$

$\sigma_\varepsilon = 1.3$

2.3   Wall Functions

Standard wall functions also known as "the law-of-the-wall" are based on the work of Launder and Spalding (1974) [19], and are widely used along with the standard $k - \varepsilon$ turbulence model for turbulent flows in industry.

2.3.1   Momentum

The wall function for near-wall mean velocity is given by:

$$U^* = \frac{1}{\kappa} \ln\left(Ey^*\right) \tag{2.18}$$

In FLUENT this wall function is only called when $y^* > 11.225$ Therefore the correct relation between near-wall velocity, U^*, and near-wall distance, y^*, is given by:

$$U^* = \begin{cases} y^* & y^* < 11.225, \\ \frac{1}{\kappa} \ln\left(Ey^*\right) & y^* > 11.225 \end{cases} \tag{2.19}$$

where U^* is the dimensionless near-wall velocity:

$$U^* \equiv \frac{U_P C_\mu^{1/4} k_P^{1/2}}{\tau_w/\rho} \tag{2.20}$$

and y^* is the dimensionless near-wall distance:

$$y^* \equiv \frac{\rho C_\mu^{1/4} k_P^{1/2} y_P}{\mu} \tag{2.21}$$

and

$\kappa =$ von Kàrmàn constant ($= 0.418$)

$k_P =$ turbulent kinetic energy at the first near-wall node P

$E =$ empirical constant ($= 9.793$)

$U_p =$ mean velocity at the near-wall node P

y_P = distance from point P to wall

μ = fluid dynamic viscosity

2.3.2 Energy

Heat Transfer through a wall is implemented using the .

$$T^* \equiv \frac{(T_w - T_p)\rho C_p C_\mu^{1/4} k_P^{1/2}}{\dot{q}} \tag{2.22}$$

$$T^* \equiv \begin{cases} \Pr y^* + \frac{1}{2}\rho\Pr\dfrac{C_\mu^{1/4} k_P^{1/2}}{\dot{q}}U_P^2 & y^* < y_T^*, \\ \Pr_t\left[\dfrac{1}{\kappa}\ln\left(Ey^*\right) + P\right] + \frac{1}{2}\rho\dfrac{C_\mu^{1/4} k^{1/2}}{\dot{q}}\left[\Pr_t U^2 + \left(\Pr - \Pr_t\right)U_c^2\right] & y^* > y_T^* \end{cases} \tag{2.23}$$

where P is defined in [19] as:

$$P = \frac{\pi/4}{\sin\left(\pi/4\right)}\left(\frac{A}{k}\right)^{\frac{1}{2}}\left(\frac{\Pr}{\Pr_t} - 1\right)\left(\frac{\Pr_t}{\Pr}\right)^{\frac{1}{4}} \tag{2.24}$$

where:

k_P = turbulent kinetic energy at the first near-wall node P

κ = von Kàrmàn constant (= 0.418)

ρ = density of fluid

$\dot{q}$ = wall heat flux

T_p = fluid temperature at the first near-wall node P

T_w = wall temperature

Pr = Prandtl number $(\mu c_p/k_f)$

Pr_t = turbulent Prandtl number (= 0.85)

A = Van Driest constant (= 26)

U_c = mean velocity magnitude at $y^* = y_T^*$

Heat transfer through wall is calculated by first solving for T^* using equation (2.23) then solving for $\dot{q}$ using equation (2.22).
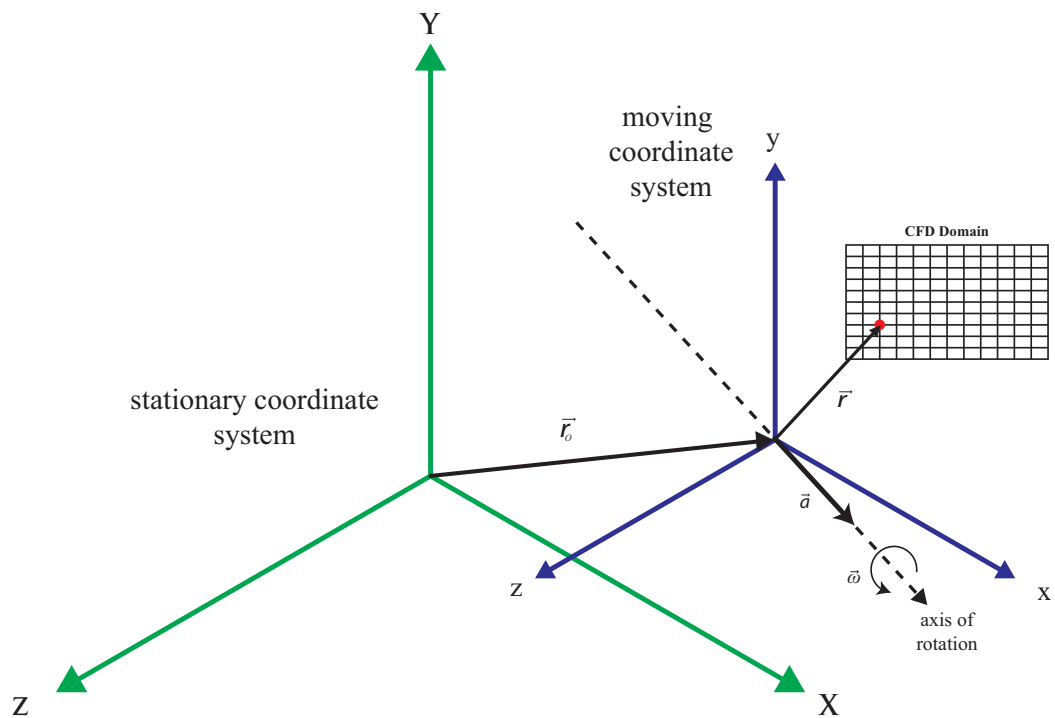
2.4 Moving Reference Frames

Figure 2.1. A diagram of a moving reference frame defined with respect to the stationary reference frame.

The final analyses presented in this thesis contains domains of air in both rotating and stationary reference frames. By default, FLUENT solves the fluid flow equations in the stationary (or inertial) reference frame. However, for some analyses it becomes advantageous to solve the equations in a moving (non-inertial) reference frame. In the

case of this thesis, the moving reference fame formulation is used to model a rotor-stator problem. The domain of air surrounding the rotor is modelled in a rotating reference frame while the stator is modelled in the stationary reference frame. An interface between the domains converts air from one reference frame to the other (see the Section 2.5 for details).

For a frame of reference rotating with angular velocity $\vec{\omega}$ and linear velocity $\vec{v_t}$ with origin of the reference frame located at position vector $\vec{r_0}$ with respect to the inertial frame, the fluid velocities can be transformed from the stationary frame to the moving frame using the following relation:

$$\vec{v_r} = \vec{v} - \vec{u_r} \tag{2.25}$$

where

$$\vec{u_r} = \vec{v_t} + \vec{\omega} \times \vec{r} \tag{2.26}$$

In these equations, $\vec{v_r}$ is the velocity relative to the moving reference frame, $\vec{v}$ is the absolute velocity, $\vec{u_r}$ is the velocity of the moving frame with respect to the stationary frame, $\vec{v_t}$ is the translational velocity, $\vec{\omega}$ is the angular velocity, and $\vec{r}$ is a position vector from the origin of the moving frame to some point in the CFD domain. See Figure 2.1

2.5   The Mixing Plane

The mixing plane model is an interface that allows flow from one frame of reference to another. In this thesis, the mixing plane is used as an interface between a rotating rotor domain and a fixed stator domain, where the rotor is upstream. The mixing plane circumferentially averages the flow parameters at the rotor exit and stator inlet, creating a radial profile of all parameters at the interface. These profiles are then set as equivalent boundary conditions for the rotor exit and stator inlet domains. This allows both domains to be solved as a steady state analysis.
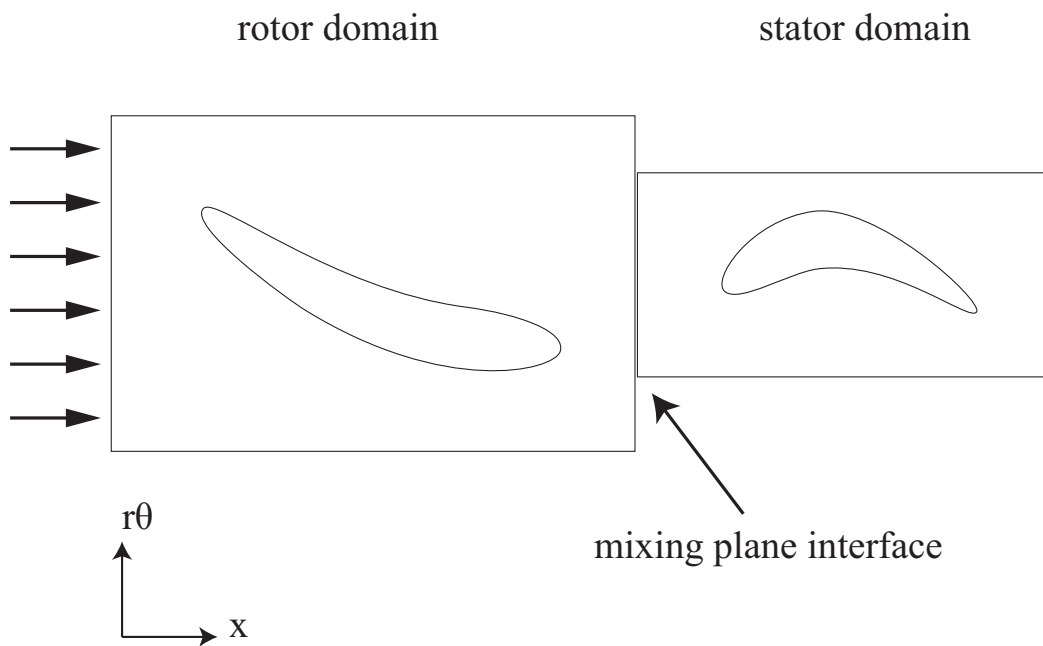

Figure 2.2.   Two grids with non-coincident nodes can be joined with an interface

2.6 Non-Conformal Interface

A non-conformal interface allows flow information to pass between two grids that do not necessarily have coincident nodes. The only requirement is that the two meshes overlap either partially or completely. See Figure 2.3 below.
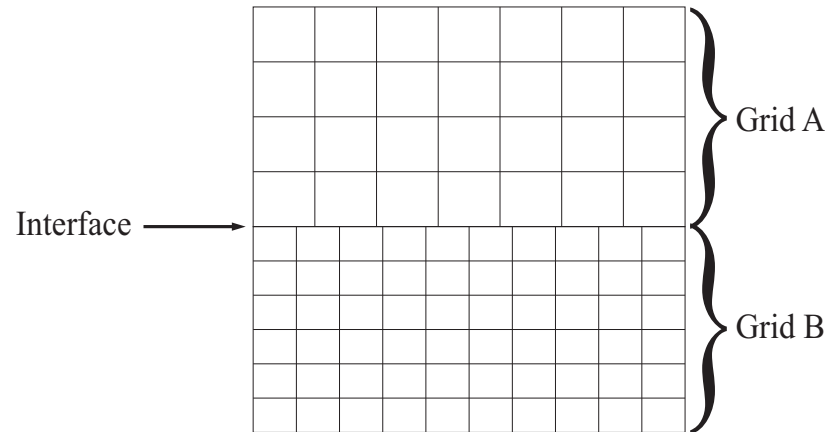

Figure 2.3. Two grids with non-coincident nodes can be joined with an interface

2.7   The SC03 Finite Element Code

Sc03 is a finite element heat conduction and structural solver developed internally by Rolls-Royce Inc. The present study is only concerned with solving metal temperatures, not deflection or stress, so only a description of temperature prediction will be given. For conduction through an isotropic solid SC03 solves the differential form of Fourier's law of heat conduction given by:

$$k\frac{\partial q_i}{\partial x_i} + \dot{q} = \rho C_v \frac{\partial T}{\partial t} \tag{2.27}$$

where ρ is metal density, C_v is specific heat, k is thermal conductivity, and q_i is the heat flux vector given by:

$$q_i = -k\frac{\partial T}{\partial x_i} \tag{2.28}$$

For this thesis none of the models have internal heat generation so equation (2.27) reduces to:

$$k\frac{\partial q_i}{\partial x_i} = \rho C_v \frac{\partial T}{\partial t} \tag{2.29}$$

The problem is then discretized in both time and space using finite time steps for time and finite elements for space. Equation (2.29) is solved by integrating over the volume of the entire domain.

$$\int_V T_1 \frac{\partial q_i}{\partial x_i} dV - \int_V \rho C_v \frac{\partial T}{\partial t} T_1 dV = 0 \tag{2.30}$$

where T_1 is any function. The first term is integrated by parts yielding:

$$\int_{\partial V} T_1 q_i dS_i - \int_V \frac{\partial T_1}{\partial x_i} q_i dV - \int_V \rho C_v \frac{\partial T}{\partial t} T_1 dV = 0 \tag{2.31}$$

The first term is an integral over the surface of the metal which depends on the model's boundary conditions. The domain V is discretized into finite elements which together form a "mesh". In SC03 each 2D element is generally a six-noded triangle, and 3D elements are usually either twenty-noded hexahedral or ten-noded tetrahedral elements. The temperature field $T(x, y, z, t)$ can be approximated by a sum over all

the elements in the domain of the product of the temperature at a given node times the shape function of that node:

$$T\left(x, y, z, t\right) = \sum_{i=nodes} T^i\left(t\right) N^i\left(x, y, z\right) \tag{2.32}$$

where T^i is the temperature at node i, and N^i is the shape function at node i. Shape functions take the value 1 the the node they are assigned to, and interpolate to 0 at all other nodes in the element. T_1 is likewise approximated the same way:

$$T_1\left(x, y, z, t\right) = \sum_{j=nodes} T_1^i\left(t\right) N^j\left(x, y, z\right) \tag{2.33}$$

the heat flow field q_j can be written as:

$$q_j\left(x, y, z, t\right) = -\sum_{i=nodes} kT^i\left(t\right) \frac{\partial}{\partial x_j} N^i\left(x, y, z\right) \tag{2.34}$$

Equations (2.32), (2.33), and (2.34) can be substituted into equation (2.31) to give:

$$\sum_{j,k=nodes} kT^j \int_V \frac{\partial N^k}{\partial x_i} \frac{\partial N^j}{\partial x_i} dV = \sum_{j,k=nodes} \rho C_v \frac{\partial T^j}{\partial t} \int_V N^j N^k dV$$
$$+ \sum_{j,k=nodes} T^j \int_{\partial V} kN^k \frac{\partial N^j}{\partial x_i} dS_i \tag{2.35}$$

T_1^j is a general function which is arbitrary, so it was set to 1. Equation (2.35) can be written in matrix form as:

$$C\frac{\partial T}{\partial t} + KT = B \tag{2.36}$$

where:

$$K = \sum_{j,k=nodes} \int_V k\frac{\partial N^k}{\partial x_i} \frac{\partial N^j}{\partial x_i} dV \tag{2.37}$$

$$C = \sum_{j,k=nodes} \int_V \rho C_v N^j N^k dV \tag{2.38}$$

$$B = \sum_{j=nodes} \int_{\partial V} kN^j \frac{\partial N^k}{\partial x_i} dS_i \tag{2.39}$$

Between time steps, temperature $T(t)$ is linearly interpolated:

$$T(t) \approx T_1 + (t - t_1)\frac{\partial T}{\partial t} \tag{2.40}$$

where:

$$\frac{\partial T}{\partial t} = \frac{T_2 - T_1}{t_2 - t_1} \tag{2.41}$$

Or, written in terms of non-dimensional time: θ

$$T = T_1 + \theta(T_2 - T_1) \tag{2.42}$$

where:

$$\theta = \frac{t - t_1}{t_2 - t_1} \tag{2.43}$$

substituting into equation (2.36) yields:

$$T_2\left(K\theta + \frac{C}{t_2 - t_1}\right) = B + T_1\left(\frac{C}{t_2 - t_1} - K(1 - \theta)\right) \tag{2.44}$$

If the boundary conditions are functions of temperature then equation (2.44) is non-linear, so it is solved using a Newton-Raphson method, where equation (2.44) is rearranged to form a residual.

$$R(T_2) = B + \frac{C}{t_2 - t_1}(T_1 - T_2) - K[T_1(1 - \theta) + T_2\theta] \tag{2.45}$$

$R(T_2) = 0$ is solved by:

$$R^{n+1} = R^n - \left(\frac{\partial R^n}{\partial T_2}\right)^{-1} R \tag{2.46}$$

where $\frac{\partial R^n}{\partial T_2}$ is given by:

$$\frac{\partial R}{\partial T_2} = \frac{\partial B}{\partial T_2} - \frac{C}{t_2 - t_1} - \frac{\partial K}{\partial T_2}[T_1(1 - \theta) + T_2\theta] - K\theta \tag{2.47}$$

In SC03 the derivatives of C and K with respect to T_2 are ignored so, (2.47) is given by:

$$\frac{\partial R}{\partial T_2} = \frac{\partial B}{\partial T_2} + \frac{C}{t_2 - t_1} - K\theta \tag{2.48}$$

Then equation (2.46) is iterated until the residuals are below a user-defined value. Once the new temperatures are solved, the boundary conditions are updated and the next time-step is solved. The steady state problem is solved using the same approach. The solution is time-stepped until metal temperatures converge.

2.7.1 SC03 Boundary Conditions

The most commonly used boundary conditions in SC03 are the stream, void, duct, convecting zone, and prescribed heat flux. All of these boundary conditions can be functions of engine parameters and conditions such as mass flow, shaft speed, air temperature, pressure etc.

The stream is perhaps the most heavily used boundary condition in conventional thermo-mechanical finite element modelling. A stream represents a given mass flow of air over the metal surface with exchanges energy with the metal through advection. The user inputs to the stream are mass flow, initial temperature, pressure, and heat transfer coefficient. A stream also allows the air to accept additional heat from another source such as windage (viscous heating).

Ducts are special cases of streams which can exchange energy with each other across the space between them. It is essentially a single stream flowing over two segments of geometry simultaneously. However, unlike streams, ducts can have different heat transfer coefficients on different segments of geometry such as laminar pipe flow.

A void is air in equilibrium with its surroundings. This boundary condition is a function of heat transfer coefficient, power, and pressure. It is generally used when the air is mostly static, with little thermal variation throughout the fluid.

The prescribed heat flux is simply a metal boundary condition with a user specified amount of heat flux. The convecting zone is a special case of the prescribed heat flux boundary condition where the flux is defined by a heat transfer coefficient and a fluid temperature. Neither of these boundary conditions are frequently used in traditional thermo-mechanical engine modelling. However, the convecting zone is used in the coupling process to define the heat flux calculated from the CFD code.

A cycle definition in SC03 is defined by ramp points and ramps that connect the points, see Figure 2.4. Each ramp point is defined by a condition number in SC03. This condition number has any number of environmental parameters associated with it such as altitude, air density, diffuser exit air temperature, shaft speed, etc. The
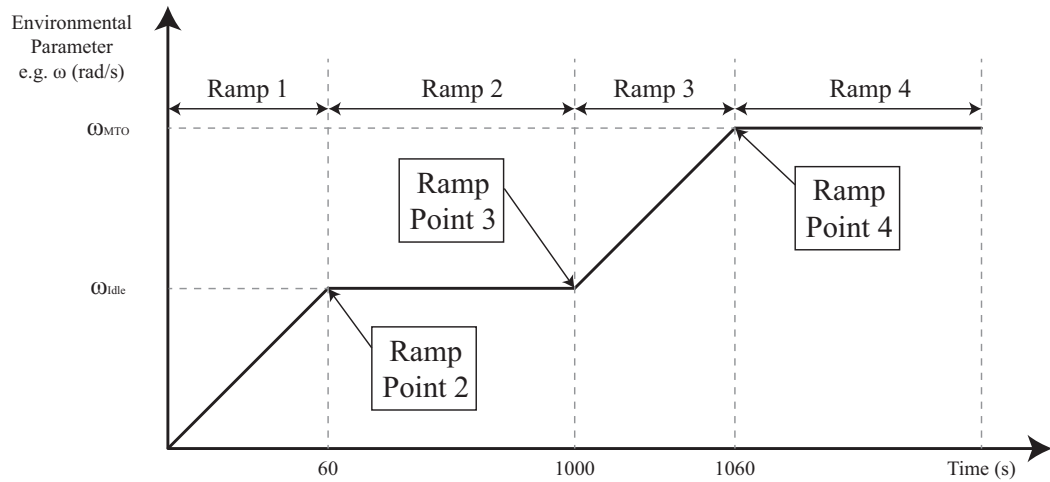
Figure 2.4. Ramps and Ramp Points in SC03

boundary conditions in SC03 are then defined by the environmental parameters at the current time point in the analysis. If the analysis is at a time point between to ramp points defined by different condition numbers, the environmental parameters are linearly interpolated between the ramp points.

2.7.2   Thermal-Fluid Coupling

The coupling of CFD and FEA codes is performed by a plugin to SC03 known as SC89. SC89 was developed to replace conventional SC03 boundary conditions with boundary conditions that exchange information with CFD, for regions where the fluid flow adjacent to the metal is not well known. The coupling plugin is capable of running 2D FE - 2D CFD, 2D FE - 3D CFD, and 3D FE - 3D CFD models. For the 2D FE - 3D CFD case, the CFD heat flux is circumferentially averaged to create a 2D profile that is written out for use by the 2D FE model. For all analyses the CFD model is fully converged for the engine condition of interest (e.g. shaft speed, altitude etc.) before the coupling analysis begins. Fluent was used as the CFD solver for all analyses in this thesis. Nearly all coupling analyses are run transiently, even if a steady state result is desired. To be more precise, the finite element analysis is

run transiently. The CFD analysis, however, is steady state. This proceeds from the observation that the fluid in an engine responds nearly instantaneously with respect to the metal. At each time point in the analysis metal temperatures from the finite element code are passed to Fluent as a continuous temperature profile. The CFD code then applies this temperature profile as a boundary condition and runs a user-specified number of iterations. The heat flux calculated at the boundaries is then passed back to the finite element solver (SC03) in the form of a heat transfer coefficient and a fluid temperature. SC03 then solves this problem and the iterative process continues until all of the metal temperatures at the boundaries converge. When the temperatures converge, SC03 proceeds to the next time step, the boundary conditions are updated, and the iterative coupling process continues. See Figure 2.5.
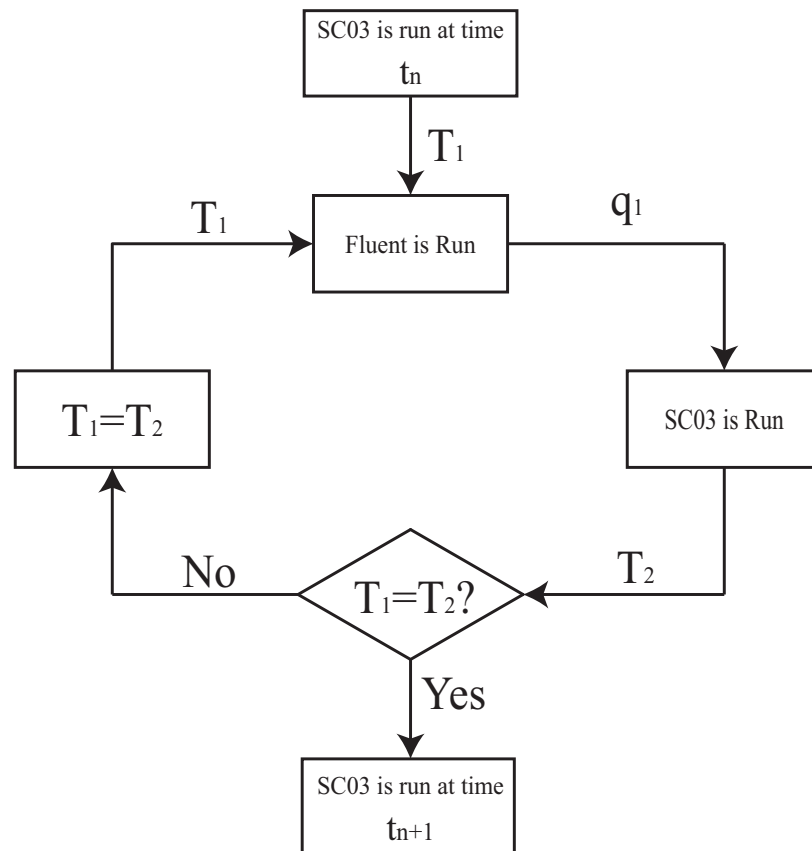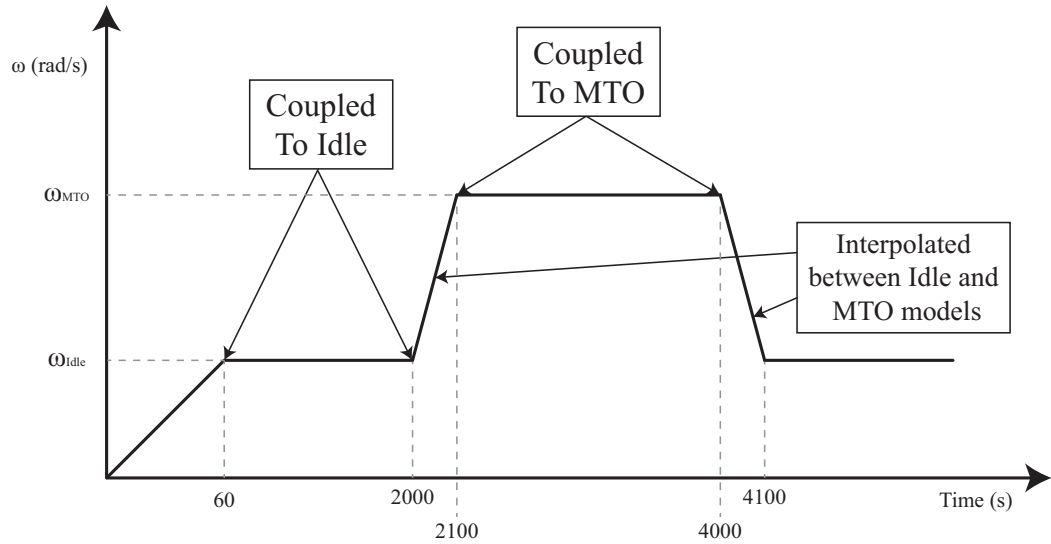

Figure 2.5. SC89 Procedure

Figure 2.6. Typical Square Cycle Definition coupled with CFD models by SC89

Each ramp point in SC03 is coupled with a specified, fully converged CFD model. Coupling analyses are typically run with a "square cycle," see Figure 2.6, where the engine accelerates to the idle condition from rest, then accelerates to the max-takeoff (MTO) condition, and finally decelerates back to idle. The coupling procedure is often run with these types of abbreviated cycle definitions because it is too computationally expensive to simulate an entire test flight with a coupled analysis. In addition, there often exists test data for these short cycles.

For ramps that exist between ramp points defined by different condition numbers, the heat flux needs to be interpolated between two CFD models. For transient ramps, both CFD models are updated with the same SC03 wall temperatures, and both analyses are run. Then the heat fluxes from both models are linearly interpolated with respect to time to calculate the heat flux as the given time point. See Figure (2.7)

The heat flux at time t is calculated by:

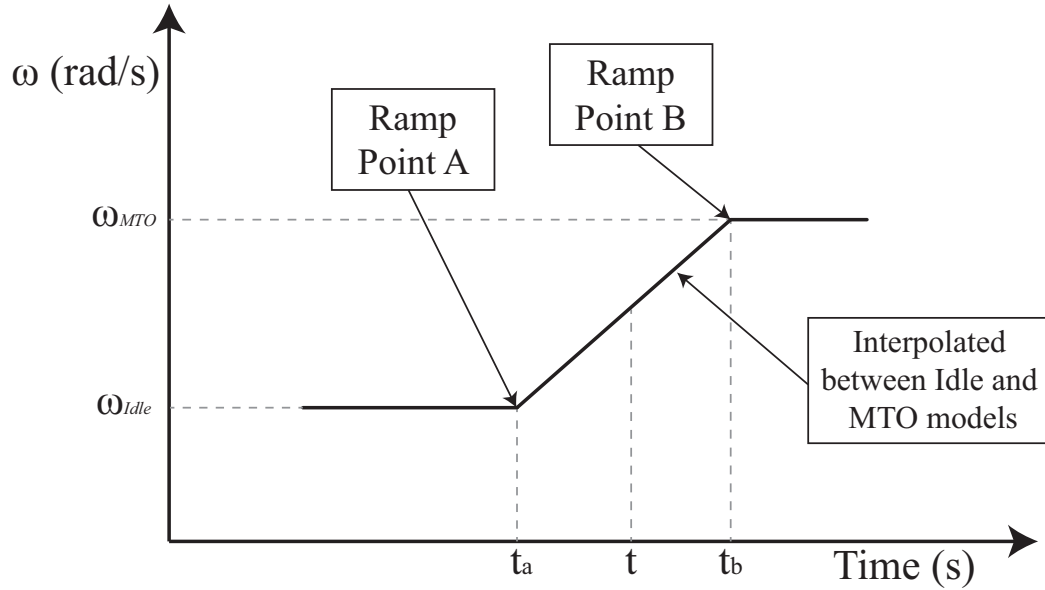$$q_t = \frac{q_b \times (t - t_a) + q_a \times (t_b - t)}{t_b - t_a} \tag{2.49}$$

Figure 2.7. Transient Ramp Interpolation

Time and resource constraints prohibited the running of even these short cycle defini-
tions in this thesis. Because MTO temperatures are the most important as it relates
to life calculations, it was decided that only steady state MTO temperatures would
be calculated. To speedup the transient analysis to reach steady state results more
quickly, the first three ramp points are coupled to NULL CFD models, Figure 2.8. A
NULL CFD model returns the following result in the convective heat flux boundary
condition:

T_f = The currently defined SC03 metal temperature

$h = 0.$

Thus a NULL model is equivalent to an adiabatic boundary condition.

The SC03 boundary condition, *convecting zone*, is used by the SC89 plugin to pass
heat flux from Fluent to the SC03 solver in the form of a heat transfer coefficient and
a fluid temperature. The method for solving a new heat transfer coefficient for each
time step is the same as in Section 1.2.1. To determine the heat transfer coefficient for
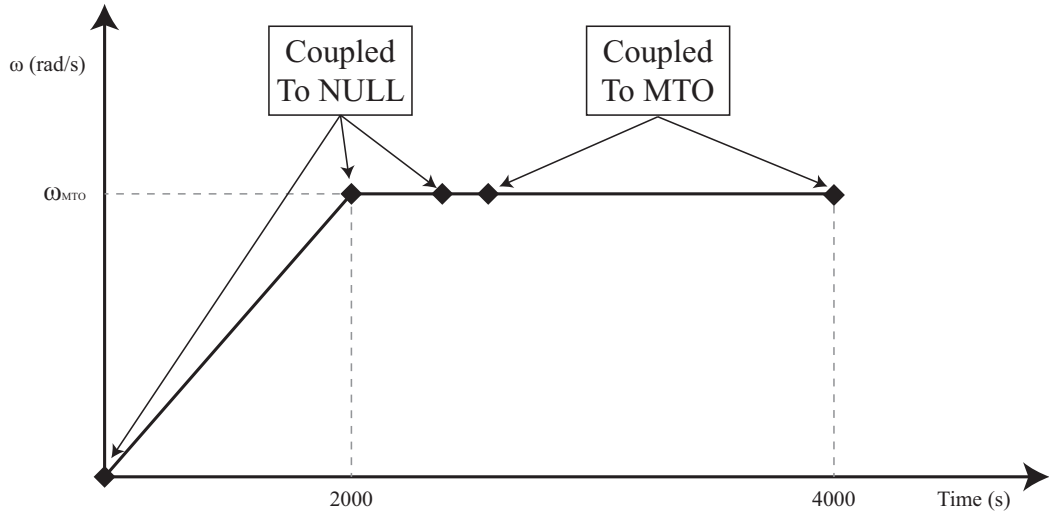a new time step, two CFD analyses are run. For the first, the CFD wall temperatures

Figure 2.8. Cycle Definition for Achieving Steady State Results

are the current metal temperatures defined by SC03. The wall temperatures of the second analysis are equal to the first temperatures artificially raised by 20 K. Thus two values for heat flux are calculated by the CFD q_1 and q_2 such that:

$$q_1 = h\left(T_f - T_m\right) \tag{2.50}$$

$$q_2 = h\left(T_f - T_{m+20}\right) \tag{2.51}$$

therefore...

$$h = \frac{q_1 - q_2}{20} \tag{2.52}$$

with h known equation (2.50) is rearranged to solve for fluid temperature.

$$T_f = \frac{q_1}{h} + T_m \tag{2.53}$$

The new values for h and T_f are together passed back to SC03 and define the heat flux boundary condition.

3. MODEL SETUP

It has been shown that knowledge of boundary conditions at metal-fluid interfaces can be greatly improved if the boundary is coupled with CFD analysis as described in Section 2.7.2. Before a coupling analysis can begin, a CFD model must be set up and converged for every engine condition of interest. The first step in creating a CFD model is to "mesh" the fluid domain. That is, to divide the domain into many discrete points in space called "nodes" where the governing equations are solved. The nodes are grouped together to form "cells" or "finite elements."

A total of five CFD models and one finite element model were used in this thesis. Two of the CFD models are 2D, and the other three are 3D. The geometry for each of the CFD models originated from the actual CAD models used to design the Rolls-Royce Inc. engine being investigated. All of the meshing for the drive cone cavity was performed in ANSYS ICEM. The rotor blade and stator vane was meshed in Rolls-Royce Inc.'s proprietary, automatic, meshing software known as PADRAM. The five CFD models are:

1. 2D - no bolts

2. 3D - no bolts

3. 2D - with porous media bolts

4. 3D - with bolts and high fidelity gaspath

5. 3D - high fidelity gaspath but no bolts

3.1 The 2D No-Bolt CFD Model

The 2D CFD models consist of the drive cone cavity and a portion of the main annulus, also known as the gas-path. Some CFD models of the drive cone cavity that have been used by other researchers do not include a portion of the main annulus, however, some research suggests that ingestion from the main gas-path models the fluid flow more accurately, e.g. Mirzamoghadam and Xiao [10] and Stevens et al. [4]. The 2D CFD model is a structured hexahedral mesh created in ANSYS ICEM. The blocking for the 2D mesh is shown in Figure 3.1.
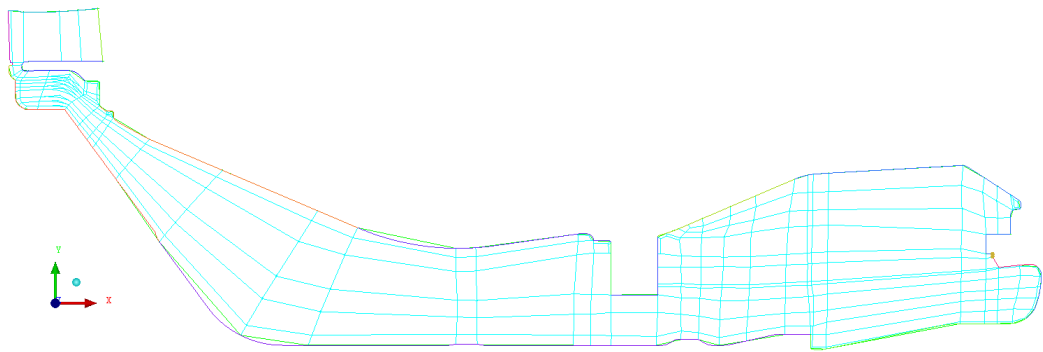
Figure 3.1. ICEM 2D Blocking
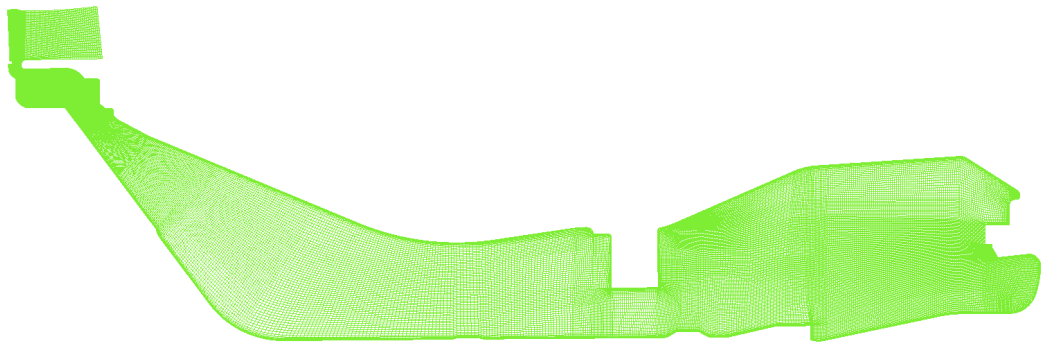
The 2D mesh is shown in Figure 3.2

Figure 3.2. 2D Mesh

This mesh contains approximately 60,000 elements.

3.1.1 Mesh Sensitivity Study

Two meshes were created from the same blocking structure, Figure 3.1, for the purpose of studying the sensitivity that mesh size and density have on the CFD analysis. The finer mesh contained approximately 135,000 elements, and the coarser mesh contained approximately 60,000 elements. A close-up of both meshes at the cavity inlet can be seen in Figures 3.3 and 3.4.
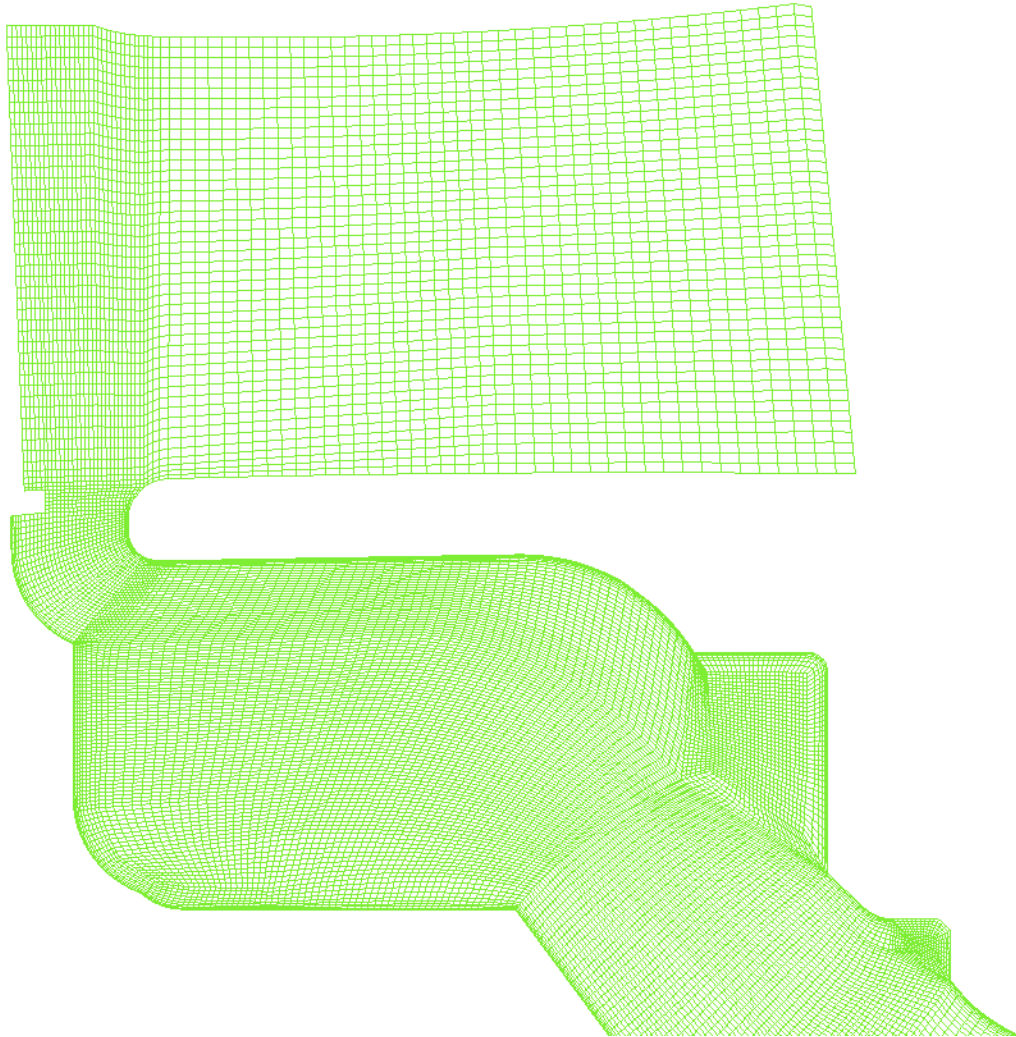

Figure 3.3. Close-up of Fine Mesh at the Cavity Inlet

The CFD model for both meshes were converged at the max take-off (MTO) engine condition. Results from both analyses were then compared to see what effect
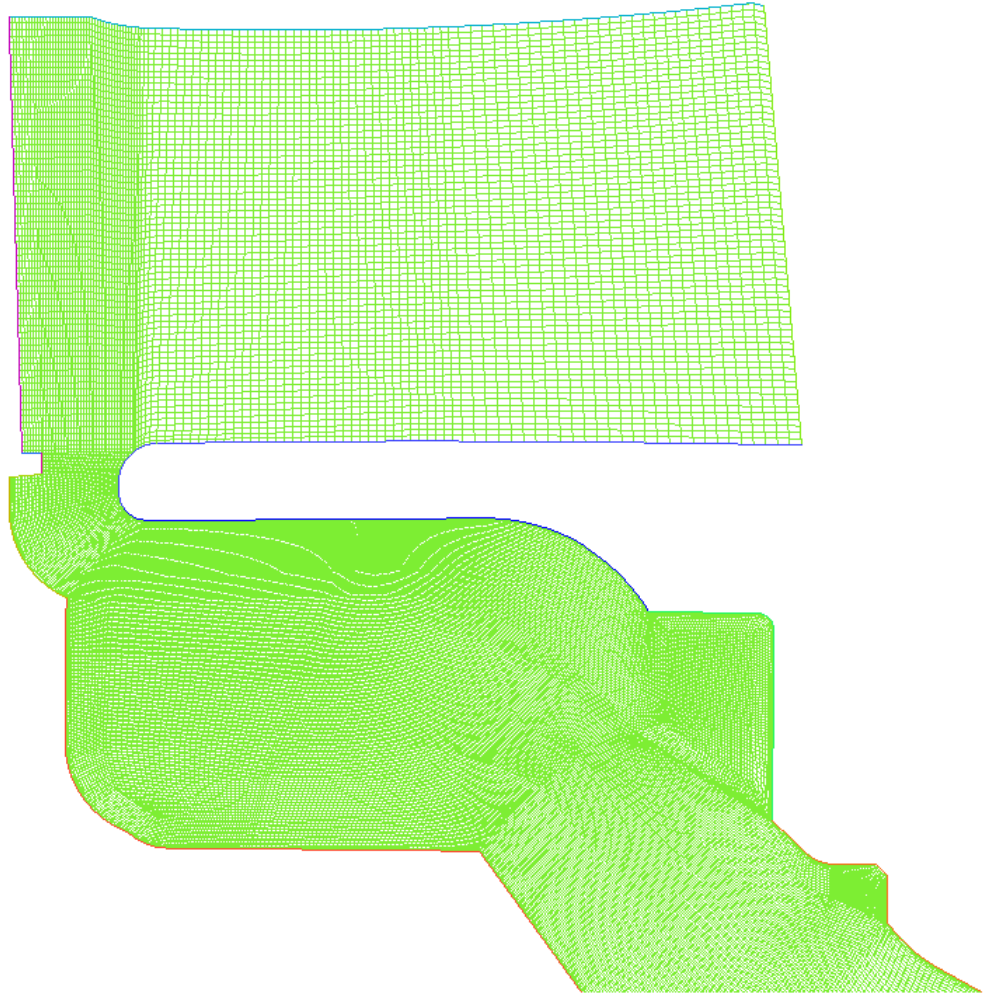
Figure 3.4. Close-up of Coarse Mesh at the Cavity Inlet

the mesh density has on the results. Figure 3.5 compares the "windage" results from both analyses. Windage is a measure of the amount of work a rotating wall puts into the fluid. It can also be considered a measure of the "viscous heating" or "frictional heating" that a wall adds to the fluid. Windage is given by the equation:

$$W = T_q \Omega = -\tau_\theta r \Omega \tag{3.1}$$

where:

τ_θ = wall shear stress in the circumferential direction

Ω = angular velocity of the wall

r = radial distance

T_q = torque per unit area

The windage in Figure 3.5 has been normalized by the correlation given by Lewis and Provins [3]:

$$W^* = \frac{W}{\rho r_0^3 \Omega^3 (r_0 \cdot a)} \qquad (3.2)$$

where r_0 is the height of the cavity, and a is the length of the cavity, see Figure 3.8.
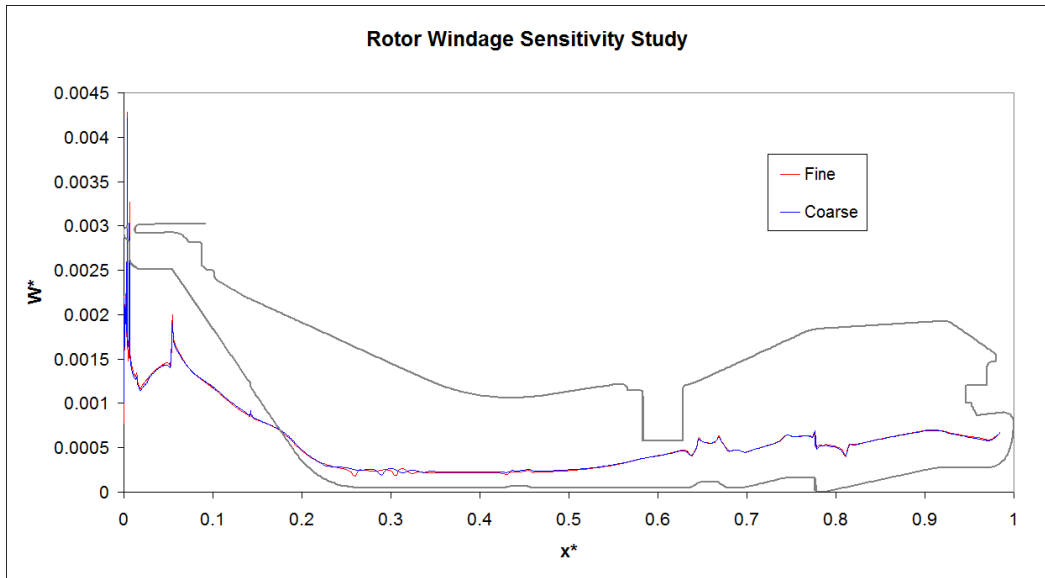

Figure 3.5.   Mesh Sensitivity Study of Rotor Windage

The two mesh densities were also compared by taking the mass average of "swirl fraction" through planes at various axial positions through the cavity, Figure 3.6. "Swirl fraction", sometimes shortened to just "swirl", is a non-dimensional measurement of circumferential velocity, given by the equation:

$$swirl = \frac{V_\theta}{r\Omega} \qquad (3.3)$$

where:

V_θ = fluid velocity the circumferential direction

Ω = angular velocity of the engine shaft

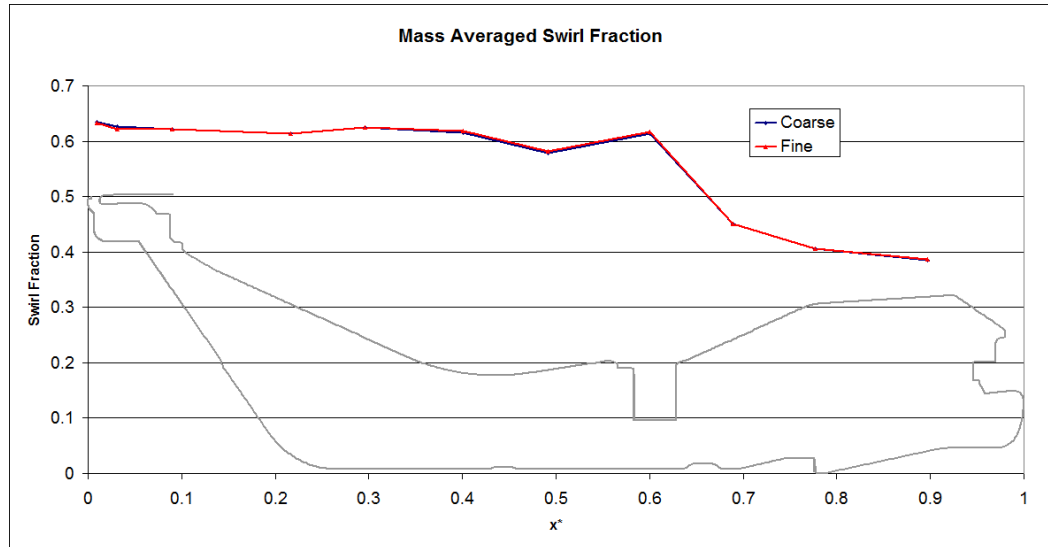r = radial distance to fluid particle

Figure 3.6.   Mesh Sensitivity of Mass Averaged Swirl Fraction

The mesh sensitivity was also compared by plotting the radial profile of various non-dimensional parameters along an axial plane in the center of the cavity (axial plane P_A in Figure 3.8), including normalized temperature in Figure 3.7(a), normalized pressure in 3.7(b), swirl fraction in 3.7(c), and normalized axial velocity in 3.7(d).

(a) Total Temperature

(b) Pressure

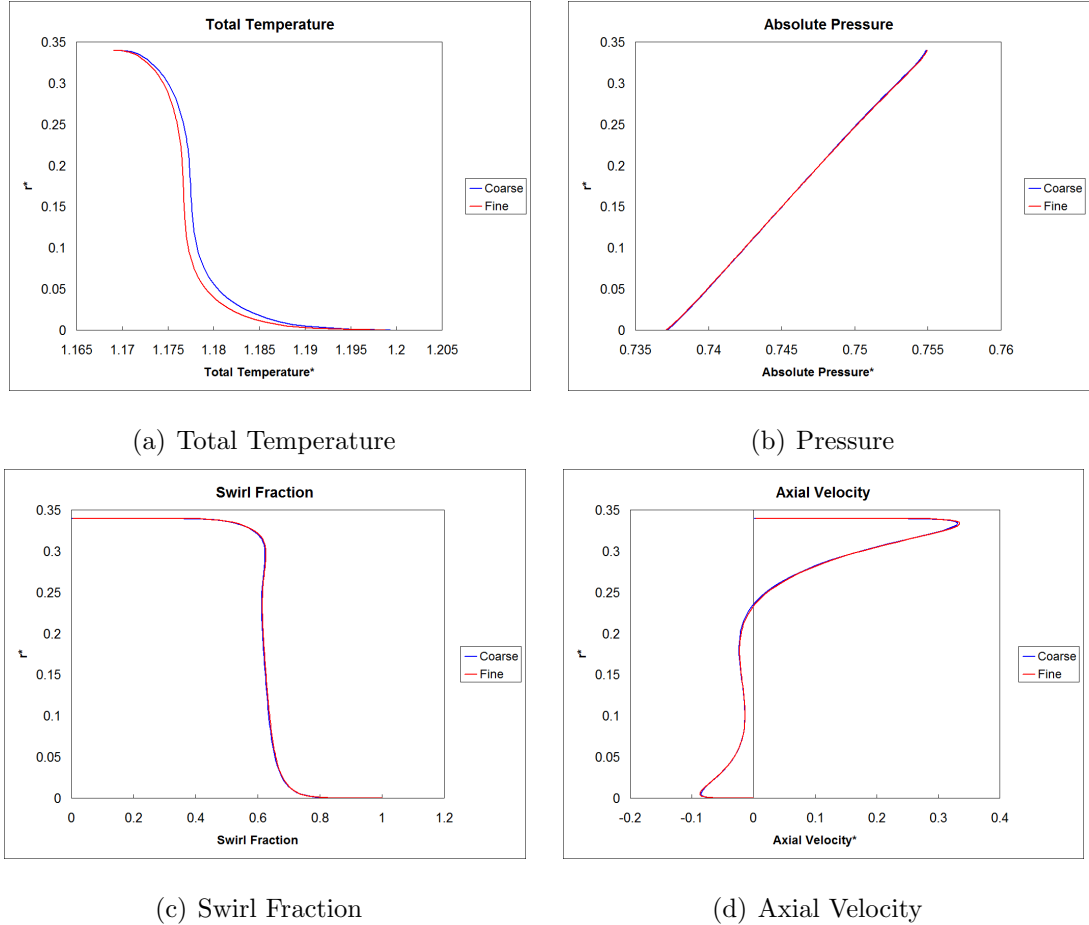(c) Swirl Fraction

(d) Axial Velocity

Figure 3.7.   Radial Profile Sensitivity of Various Flow Parameters

Temperature and pressure have been normalized by the HP system, Figure 1.1, inlet and exit temperature and pressure. The HP system inlet temperature and pressure are known as T_{26} and P_{26} respectively. Likewise, the HP system exit temperature and pressure are known as T_{30} and P_{30} respectively, Figure 3.8. Normalized temperature and pressure are given by:

$$T_{total}^* = \frac{T - T_{26}}{T_{30} - T_{26}} \tag{3.4}$$

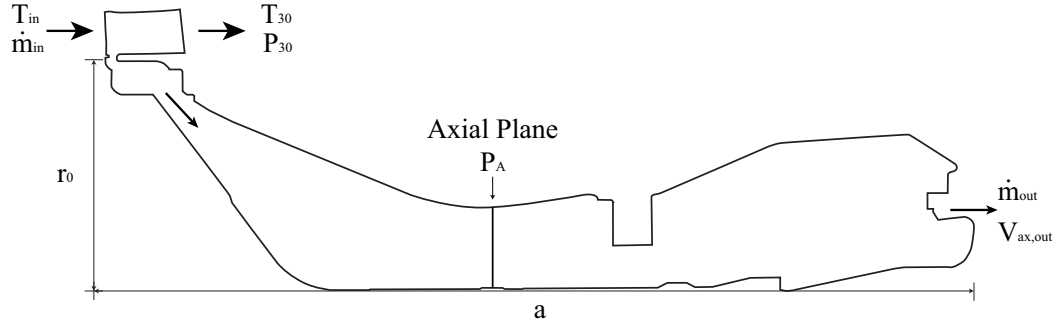$$P_{abs}^* = \frac{P - P_{26}}{P_{30} - P_{26}} \tag{3.5}$$

Figure 3.8. Diagram of Boundary Condition Parameters and Dimensions

Axial velocity has been normalized by simply dividing it by the axial velocity at the exit of the cavity ($V_{ax,out}$ in Figure 3.8). These results give a high level of confidence that the CFD analysis results are independent of mesh density for the two densities in question. Therefore the analysis can proceed with the coarser of the two mesh sizes to save computational expense. The mesh statistics are summarized below:

Expansion ratio = 1.3

Near wall spacing $\approx$ 6e-5m

Number of elements $\approx$ 60,000

3.1.2   Turbulence

No turbulence sensitivity study was done for this thesis due to time constraints. However, Verdicchio [9] performed a turbulence model sensitivity study for a similar drive cone cavity with a 2-layer model and a standard $k - \varepsilon$ model. He concluded

that the boundary heat flux in the $k - \varepsilon$ model matched the 2-layer model sufficiently well and with far less computational cost. Therefore, the decision was made to use the $k - \varepsilon$ turbulence model for all the analyses in the study. For this reason the $k - \varepsilon$ model is used for all of the analyses in the present study as well.

The CFD model was setup using the $k - \varepsilon$ model and standard wall functions. These wall functions require that y^+ values remain in the range: $30 < y^+ < 100$ to be effective. It is important that the wall functions are effective because the purpose of the CFD calculation in a coupling analysis is to find the heat flux at the wall. Heat flux is calculated by the wall functions. Over several iterations the analysis was converged, the y^+ values were calculated, the near wall spacing was refined, and the analysis reconverged to make sure that the y^+ values were in the correct range. Figure 3.9 shows the y^+ values from the rotor and stator walls. Except for a few outlier regions, the y^+'s are in the correct range for the wall functions to be effective.
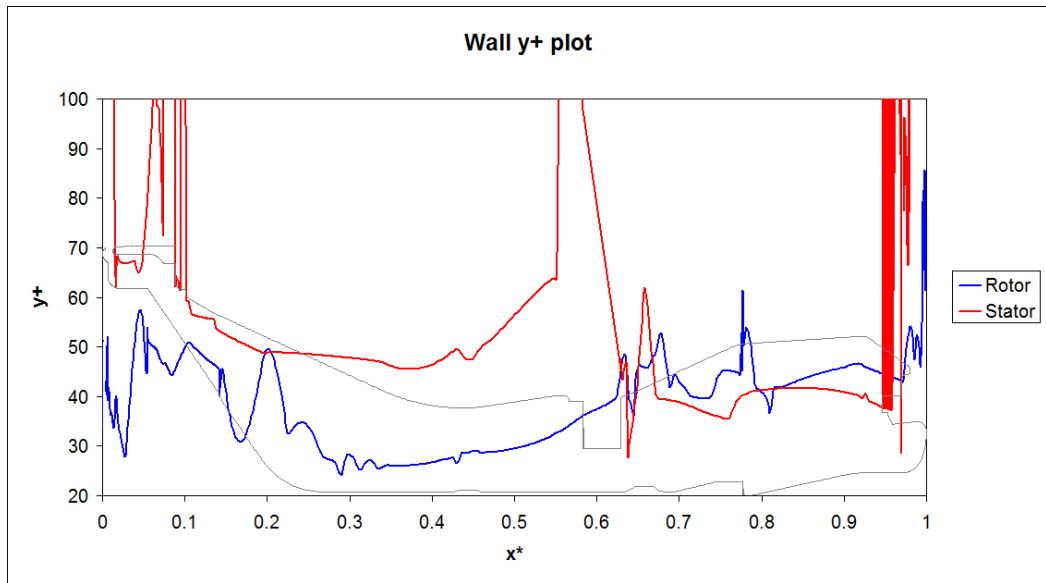

Figure 3.9. y+ Values for the Rotating and Stationary Walls in the Cavity

For the 2D CFD model, the turbulence boundary conditions were set using intensity and hydraulic diameter. Turbulent intensity, I, is defined as the ratio of the

root-mean-square of velocity fluctuations, u', to the mean flow velocity, u_{avg}. From the Fluent User Guide [17]:

$$I \equiv \frac{u'}{u_{avg}} = 0.16 \left(Re_{D_h}\right)^{-\frac{1}{8}} \tag{3.6}$$

where:

$$Re_{D_h} = \frac{\rho u D_h}{\mu} \tag{3.7}$$

and

$$D_h \equiv \frac{4A}{P} \tag{3.8}$$

for an annulus:

$$D_h = \frac{4 \cdot 0.25\pi \left(D_o^2 - D_i^2\right)}{\pi \left(D_o - D_i\right)} = D_o - D_i \tag{3.9}$$

where:

D_o = outer diameter

D_i = inner diameter

The CFD model setup for the 2D no-bolt case is setup in Table 3.1 below.

Table 3.1. Model Setup for 2D case without bolts

Solver	
precision:	single
formulation:	pressure based
pressure-velocity coupling:	SIMPLE
discretization:	second order
Model Parameters	
turbulence model:	sandard $k - \varepsilon$
wall functions:	standard
density:	ideal gas (compressible)
air definition:	piecewise-linear

3.1.3 Boundary Conditions

The temperature, pressure, and mass flow boundary conditions come from a previously setup analysis created by Rolls-Royce Inc., see DNS163600 [20]. All of these boundary conditions originated from a number of sources. The inlet temperature boundary condition, T_{in} in Figure 3.8, has been set to match thermocouple data inside the cavity. Specifically, T_{in} was set so the fluid temperature in the cavity inlet region was equal to fluid thermocouple T4389, Figure 3.10.
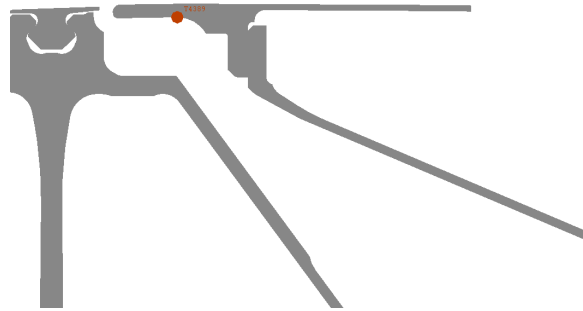

Figure 3.10. Location of Cavity Inlet Air Thermocouple

The mass flow m_{in}, temperature T_{30}, and pressure P_{30} (Figure 3.8) are all determined by the performance division of Rolls-Royce Inc. The fraction of airflow that is bled from the main gaspath to purge the drive cone cavity m_{out}, is determined by the secondary flow group by solving a one dimensional network of flow equations.

3.2 The 3D Axisymetric CFD Model

The 3D axisymetric model is simply the 2D CFD model from Section 3.1 swept into a sector. The sector size is a fraction of a circle equal to the number of HP6 rotor blades. Because the near wall spacing was maintained, the y^+'s were almost identical to those from the 2D case. Instead of solving a separate swirl equation (circumferential flow) as in the 2D case, the sector's boundary walls were defined to be rotationally periodic.
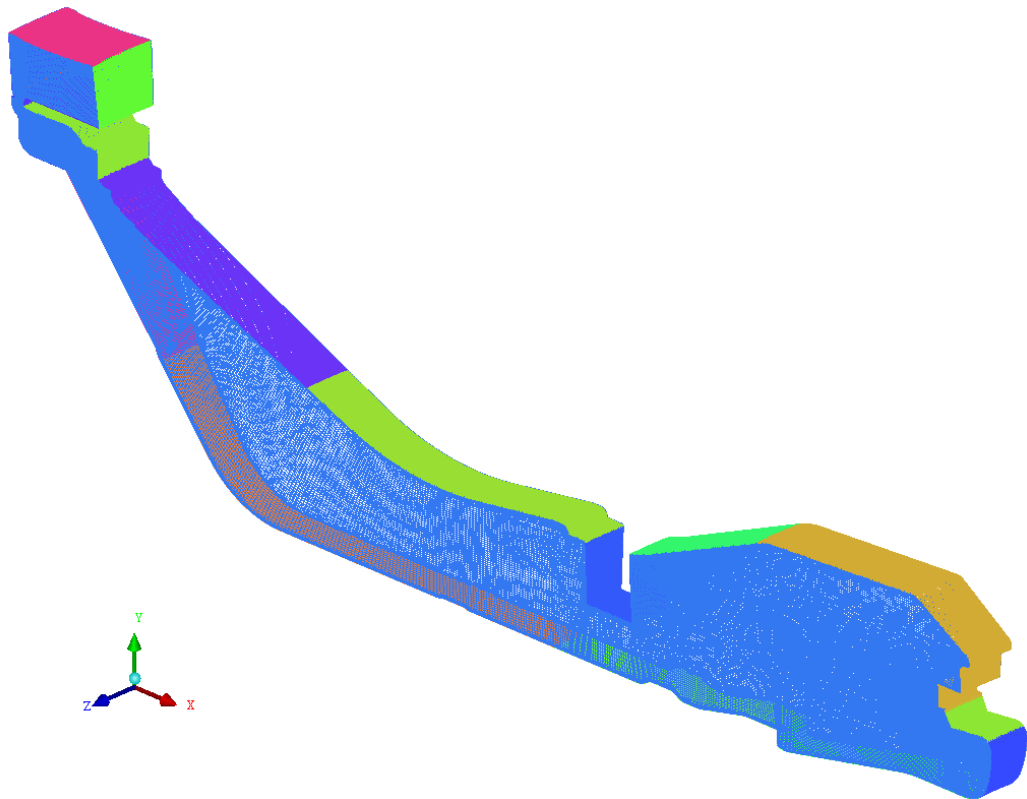

Figure 3.11. 3D Mesh Swept from 2D

The 3D sector mesh, Figure 3.11, contains approximately 2.5 million elements. All of the boundary conditions and model setup are the same as those in Section 3.1.

3.3   The 2D CFD Model with Porous Media Bolts

The 2D CFD Model with Porous Media Bolts was meshed and setup previously by Rolls-Royce Inc. which is detailed in DNS163600 [20]. Although no mesh sensitivity study was performed for this analysis, the model contains approximately the same number of cells as the mesh in the above Section 3.1. Therefore it is reasonable to assume that the analysis is mesh-independent.
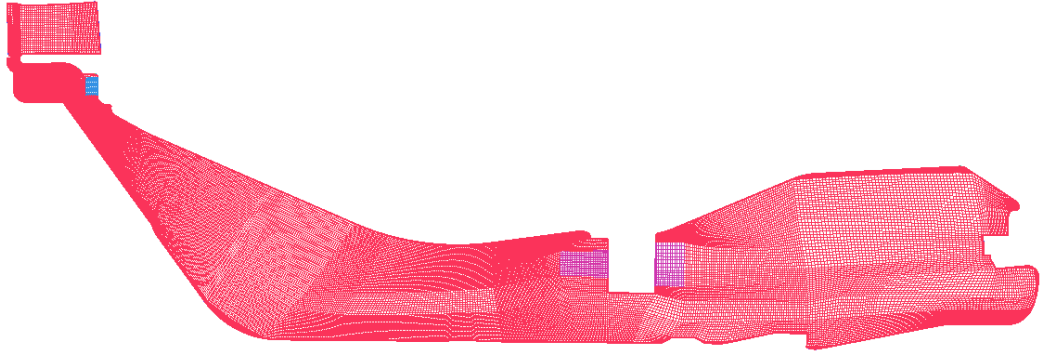

Figure 3.12.   2D Mesh with Porous Media Bolts

All of the boundary conditions are the same as those described in Section 3.1.3. However, to simulate the drag effects that the bolts have on the airflow, specific regions of the mesh were defined to have porous properties. Figure 3.12 shows the 2D mesh with the regions shown in purple defined as porous. Another Rolls-Royce Inc. study, DNS153985 [21], compared a 3D CFD analysis with 3D bolts, to a 2D CFD analysis with bolts represented by porous media. This study concluded that the drag caused by the bolts was well represented by the porous media. The porosity of the bolt region is simply defined as:

$$\gamma = \frac{Volume\,of\,the\,Fluid}{Total\,Volume} \tag{3.10}$$

3.4   The 3D CFD Model with Merged Gaspath and Bolts

The ultimate goal of this study is to determine if a high fidelity 3D CFD model is capable of predicting air and metal temperatures with greater accuracy than a 2D model. The high fidelity CFD model contains the final (sixth) stage of the HP compressor gaspath mesh, which includes the HP6 rotor, OGV, and the drive cone cavity mesh. The cavity mesh has been modified to include the flange bolts and OGV nut as well, see Figure 3.13.
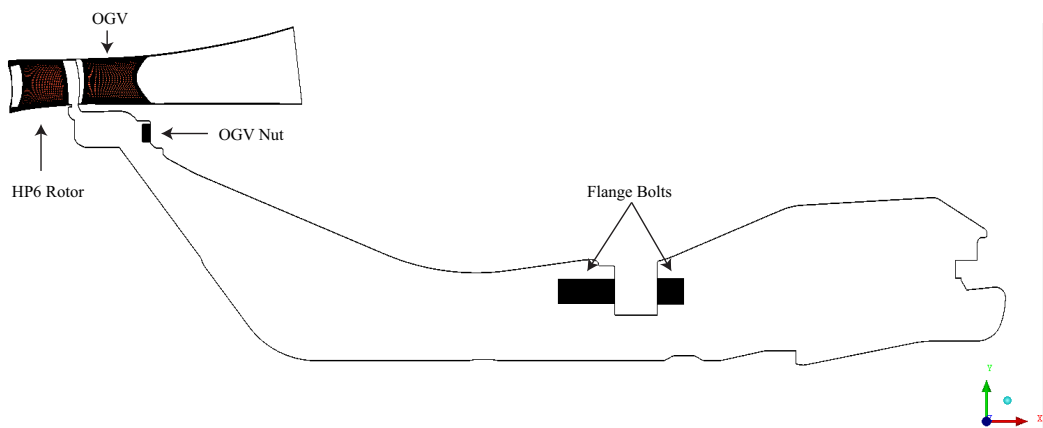

Figure 3.13.   Outline of High Fidelity 3D Model

As previously stated, all of the meshing for the drive cone cavity was performed in ANSYS ICEM. The rotor blade and stator vane, however, was meshed in Rolls-Royce's proprietary, automatic, meshing software known as PADRAM. Setting up a CFD model that contains both meshes presents a number of challenges. First of all the gaspath mesh, and the cavity mesh are radially misaligned.

This is because the rotor and stator blade meshes were created by the Compressor Aero group of Rolls-Royce Inc. to represent the geometry of the HP system, Figure 3.15, in the running condition. This is known as "hot" geometry because as the engine runs, the geometry "grows" due to thermal expansion. The geometry for the cavity, however, is designed in the "cold" position, which means the as-machined position. Thus the rotor-stator mesh is shifted radially from the cavity as shown in Figure 3.14.
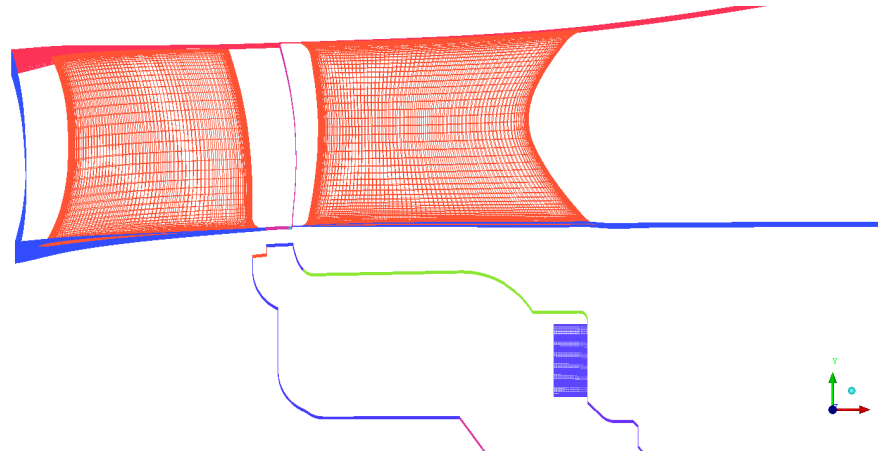
Figure 3.14.   Radial Misalignment of Hot Rotor-Stator Mesh and Cold Cavity Mesh

This challenge was addressed by radially scaling the entire rotor-stator mesh by the appropriate factor to align the meshes 3.16.

Once the two meshes were aligned, the next problem was to determine how the rotor domain and the cavity domain would share flow information between them at the interface. The first approach attempted was to use a non-conformal interface between the two grids. A non-conformal interface is a tool in Fluent that averages the flow equations at the mesh interface to pass information between the meshes even though the nodes do not coincide. Unfortunately, the high Mach numbers and turbulence at the interface caused the solution to diverge. Therefore a more robust method for joining the two meshes was needed.

The second approach was to actually merge the two meshes at the interface node by node. In order to do this, both meshes were modified so that their interfaces contained exactly the same number of nodes in both the axial and circumferential directions. The figure 3.17(a) shows the interface of both meshes before they were merged. The blue mesh is the interface of the cavity, created in ICEM. The red mesh is the interface of the rotor domain, created in PADRAM. The interface was merged node-by-node in ANSYS ICEM, thus joining both meshes into a single domain. The final merged interface is shown in Figure 3.17(b)
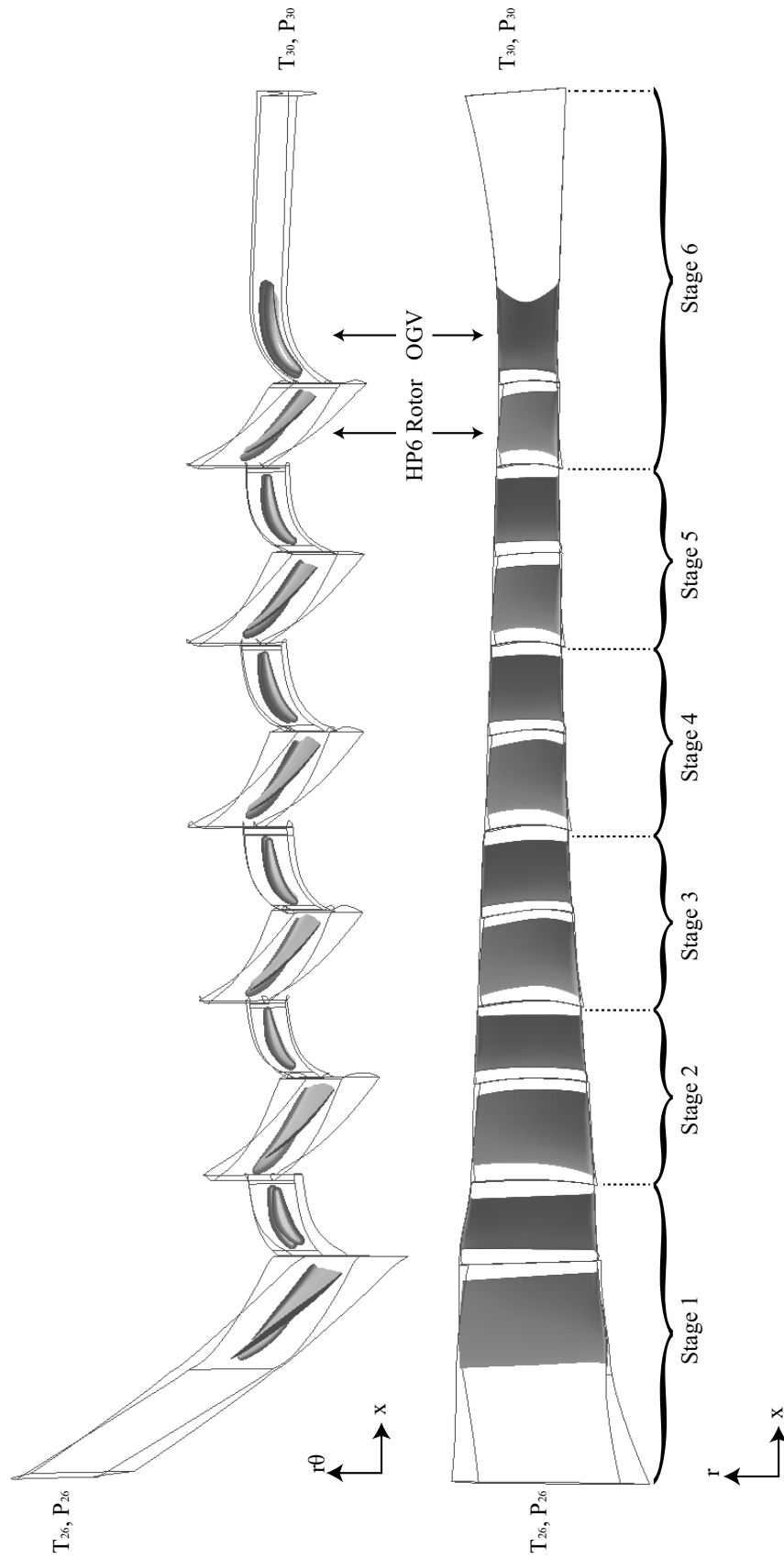
Figure 3.15. High Pressure Compressor Blades. Geometry and CFD
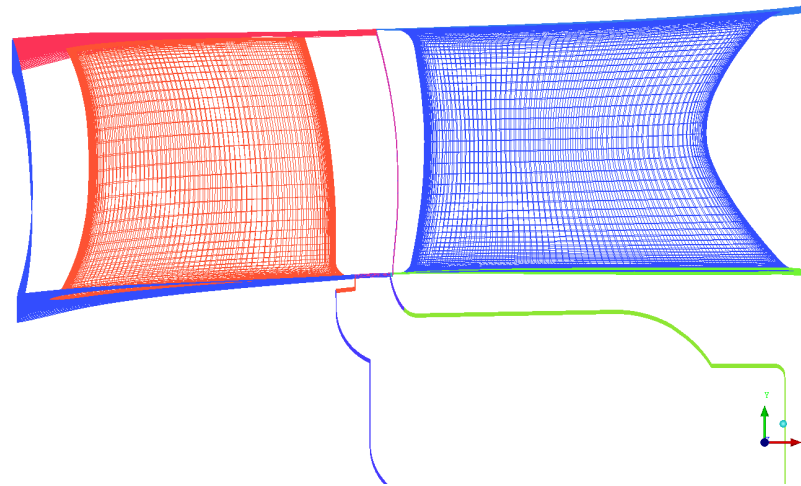Mesh Domains Created By the Compressor Aero Group.

Figure 3.16. Rotor/Stator Mesh Aligned with Cavity Mesh
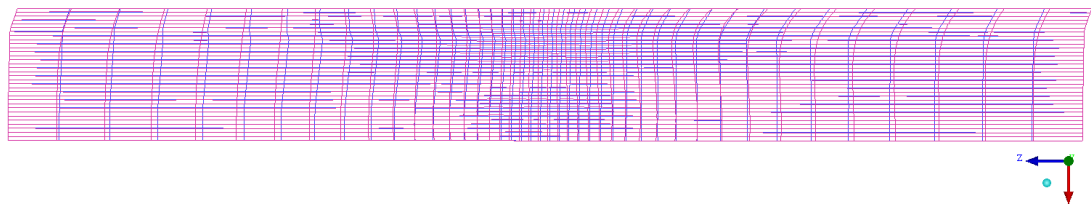
(a) Interface Meshes Before Merged
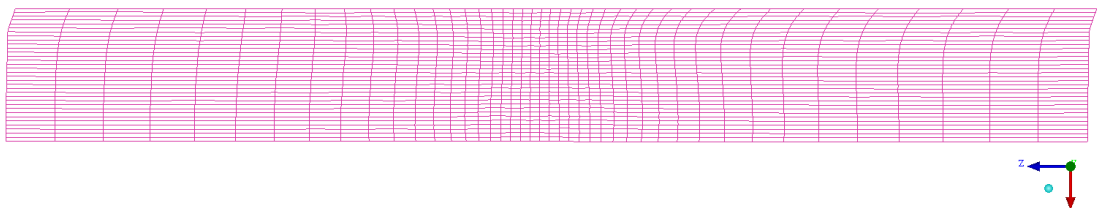
(b) Interface Mesh After Merge

Figure 3.17. Mesh Interface Before and After Merge

The 3D sector mesh was further modified by adding the flange bolts and OGV nuts, Figure 3.13. The bolts were meshed using ANSYS ICEM. The blocking for the bolts is shown in Figure 3.18. Figure 3.19 is a close up view of the mesh on the surface of the 3D flange bolts.
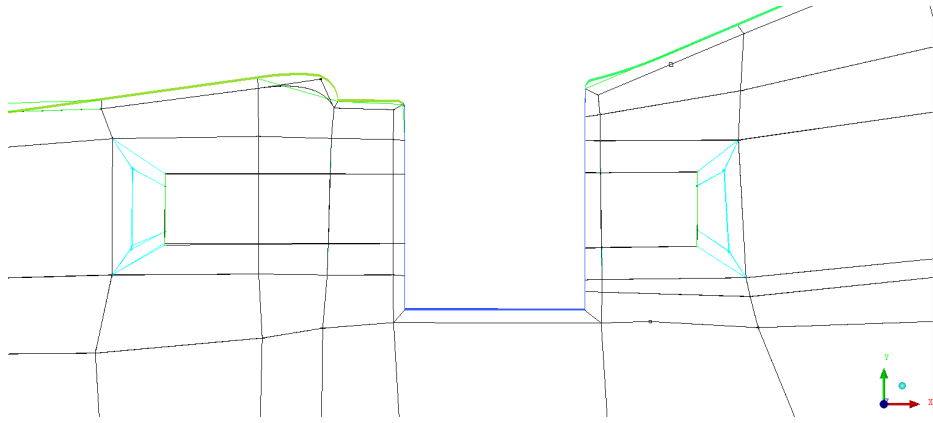
Figure 3.18.   Blocking for 3D Flange Bolts
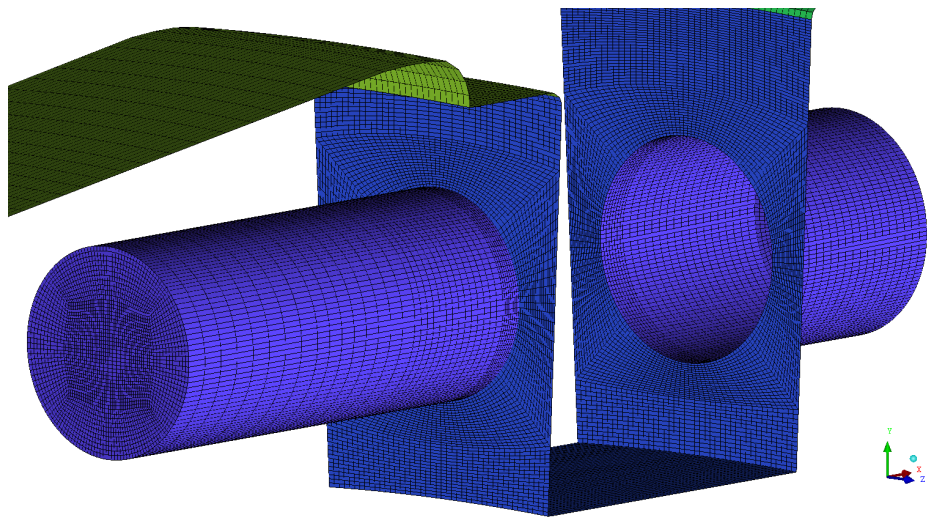
Figure 3.19.   3D Flange Bolts Mesh

A circumferential view of the blocking for the OGV nut is shown in Figure 3.20, and an axial view of the nut mesh is shown in Figure 3.21.
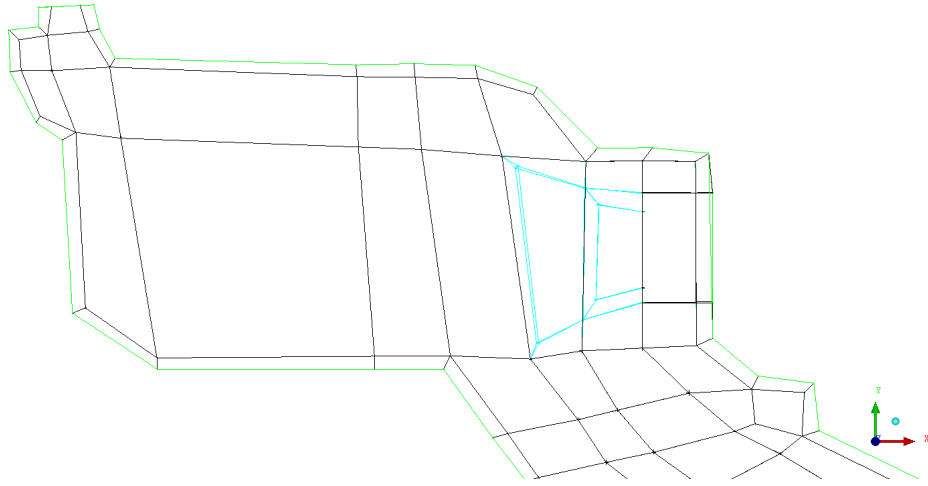
Figure 3.20. 3D OGV Nut Blocking
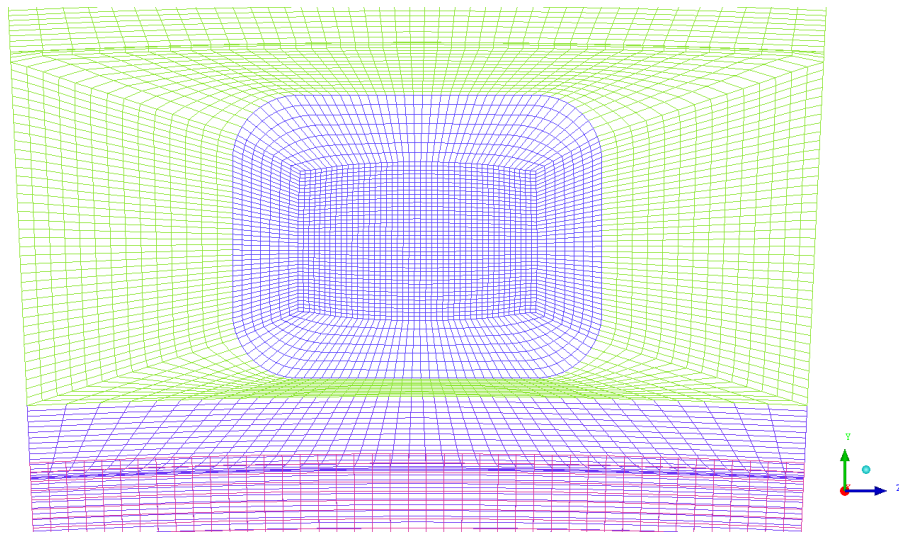
Figure 3.21. 3D OGV Mesh

For the engine of interest, the number of flange bolts does not equal the number of OGV nuts or the number of rotor blades. To minimize computational cost it is advantageous to run a sector mesh that contains only one of each of these features. The sector size was chosen such that the number of sectors per circle equals the number of rotor blades. The flange bolts and OGV nuts were then scaled in order to

maintain their drag coefficient while changing their number to equal the number of rotor blades.

$$F_d = \frac{1}{2}\rho u^2 c_d A \tag{3.11}$$

$$F_{d1} = F_{d2} \tag{3.12}$$

$$\frac{1}{2}\rho_1 u_1^2 c_{d1} A_1 = \frac{1}{2}\rho_2 u_2^2 c_{d2} A_2 \tag{3.13}$$

$$n_1 A_1 = n_2 A_2 \tag{3.14}$$

$$A_2 = \frac{n_1}{n_2} A_1 \tag{3.15}$$

where:

F_d = drag force due to the bolts

c_d = drag coefficient

u = velocity magnitude

A = bolt area

n = number of bolts
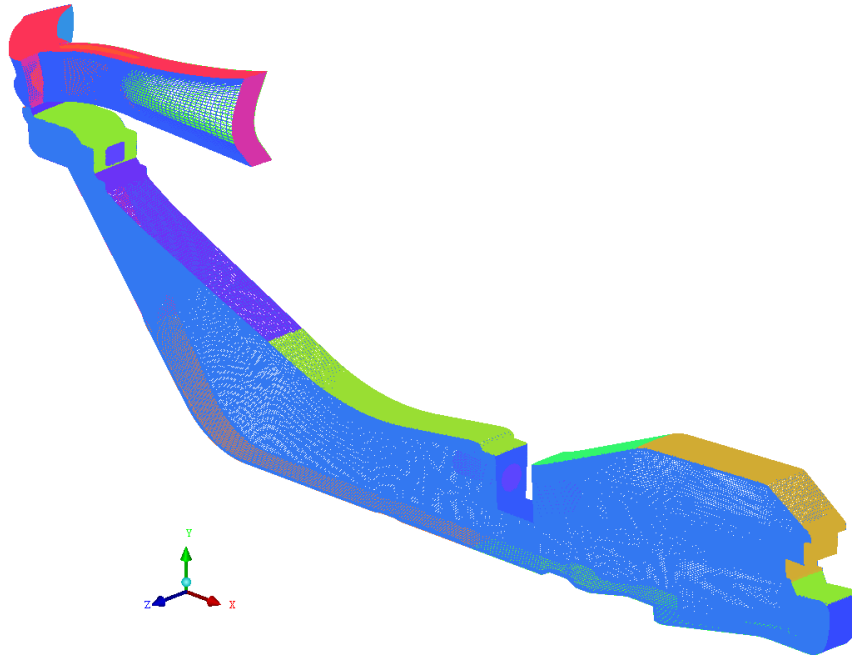
Figure 3.22. Complete 3D Sector Mesh with Merged Gaspath and Bolts

The final merged mesh is shown in Figure 3.22, and it contains approximately four million hexahedral elements.

3.4.1   The Inlet Temperature

As already mentioned, the Compressor Aero department of Rolls-Royce Inc. previously ran an analysis in which they solved the flow through the main gaspath of the HP compressor system at the engine cycle point of interest, see Section 1.3. The CFD domain of this analysis is shown in Figure 3.15. Therefore radial profiles of temperature, pressure, mass flow, turbulence, and velocity vectors at the rotor inlet and stator exit were obtained from this analysis. The normalized HP rotor inlet temperature profile is shown in Figure 3.23.

Because SC89 couples analyses transiently, it must have the ability to change the inlet temperature(s) of the CFD with time. For this reason, SC89 does not have the ability to utilize a temperature profile at the inlets. Instead, the inlet temperatures
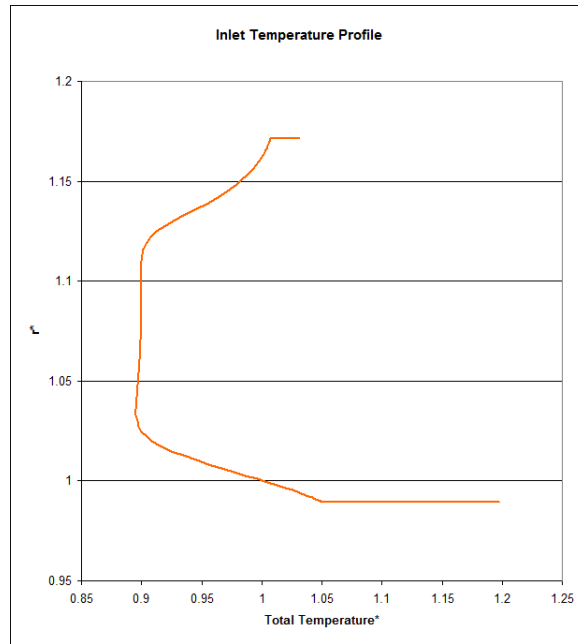
Figure 3.23.   Radial Profile of Normalized Inlet Total Temperature
to the HP6 Rotor

must be constant. Because the purpose of this study is to predict metal temperatures
in the drive cone cavity, a constant inlet temperature for the HP6 rotor inlet must be
chosen such that the air coming into the cavity is the same temperature as it would be
if the temperature profile from Aero, Figure 3.23, was being used. The air that enters
the drive cone cavity originates at some bulk radius on the HP6 rotor inlet. Once this
radius is determined, the corresponding inlet temperature can be determined from
the temperature profile.

In order to determine the inlet radius at which the bulk flow enters the cavity, a
plane at the inlet to the cavity was seeded with 500 pathlines in Fluent, which were
then tracked backwards to their origin points on the HP6 rotor inlet, Figure 3.24.

The pathlines were then saved as a Fieldview file, which gives the X,Y, and Z
location of each particle at every time step, for each pathline. A script was written
which extracts the X,Y, and Z location of each pathline where it crosses the rotor
inlet. The scatter plot in Figure 3.25 shows the origin points of each pathline on the
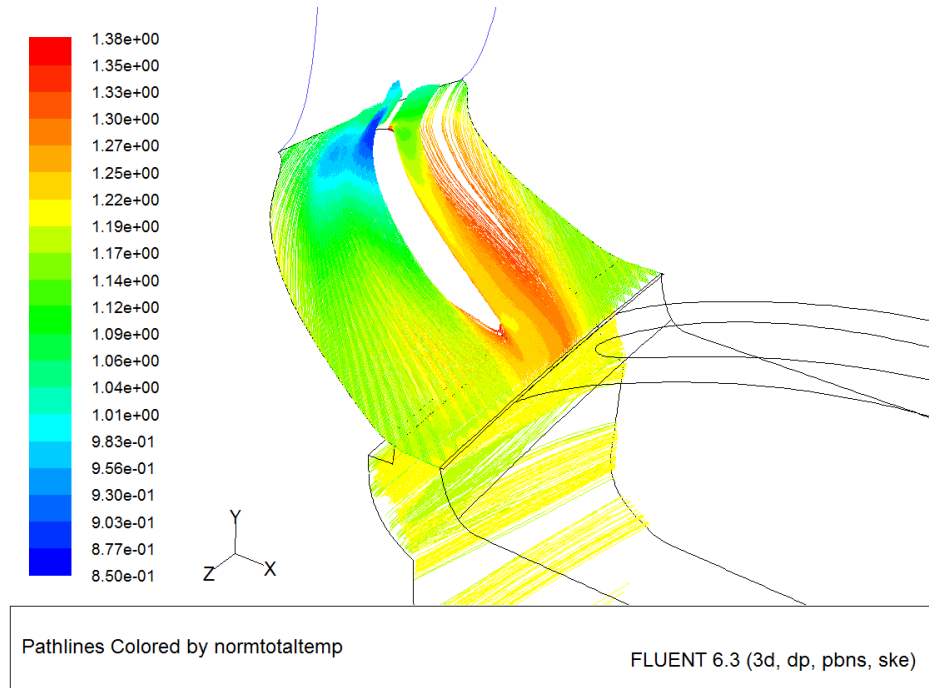
Figure 3.24. Cavity Inlet Pathline Tracking
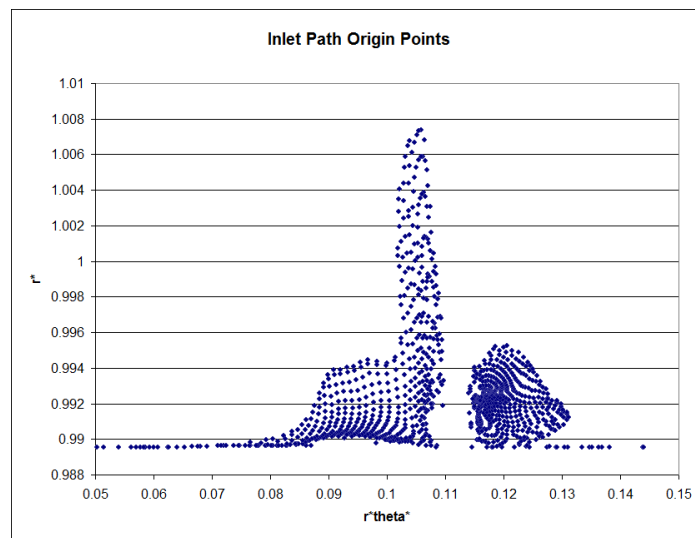
Figure 3.25. Origin of Pathlines that will Enter the Drive Cone Cavity

rotor inlet surface. In other words, streams of air that originate from these points will enter the drive cone cavity.
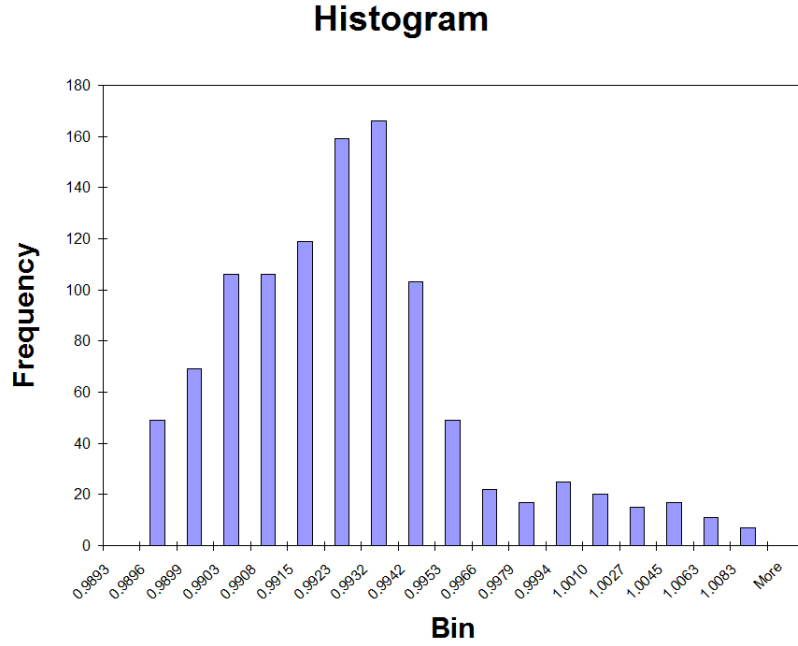
Histogram

Figure 3.26.   Origin of Pathlines that will Enter the Drive Cone Cavity

A histogram was generated from these origin points, Figure 3.26, which shows the number of particles that originate from a given radius. The bin numbers for the histogram are the same radii that the inlet temperature profile is specified by. From this histogram data, the mass-averaged inlet temperature is calculated by the following from the Fluent Theory Guide:

$$\frac{\int \phi \rho \left| \vec{v} \cdot d\vec{A} \right|}{\int \rho \left| \vec{v} \cdot d\vec{A} \right|} = \frac{\sum_{i=1}^{n} \phi_i \rho_i \left| \vec{v} \cdot d\vec{A} \right|}{\sum_{i=1}^{n} \rho_i \left| \vec{v} \cdot d\vec{A} \right|} \tag{3.16}$$

$$\frac{\int \phi \rho \left| \vec{v} \cdot d\vec{A} \right|}{\int \rho \left| \vec{v} \cdot d\vec{A} \right|} = \frac{\sum_{i=1}^{n} \phi_i \rho_i v_x r \Delta r}{\sum_{i=1}^{n} \rho_i v_x r \Delta r} \tag{3.17}$$

where:

r = radial coordinate

Δr = change in radius

ϕ = field variable

The frequency data from the histogram is then included, F_i, to give more weight to radii where more points originate. The mass-weighted average of total temperature is being found so the field variable $\phi_i = T_i$. Therefore, the mass-weighted average of total temperature at the rotor inlet is given by:

$$T_{inlet} = \frac{\sum_{i=1}^{n} T_i F_i \rho_i v_x r \Delta r}{\sum_{i=1}^{n} F_i \rho_i v_x r \Delta r} \tag{3.18}$$

All other boundary conditions at the HP6 rotor inlet and OGV exit including pressure, velocity vectors, mass flow, and turbulence were taken from the Compressor Aero analysis.

3.4.2 Reference Frames

The optimal approach for modeling flow around solid moving objects, for steady state analyses, is to put those objects in a moving reference frame such that the object is stationary with respect to that reference frame. Thus, the HP6 rotor was modeled in a moving frame of reference, rotating at the same speed as the rotor. The OGV is stationary in the absolute frame, therefore it is necessary to utilize a mixing plane, see Section 2.5, between the two domains. Because the flange bolts are also stationary in the absolute frame, they should also be modeled as such. However, it proved to be extremely difficult to place a mixing plane anywhere in the drive cone cavity due to the high degree of swirl in the cavity. As such, there was little choice but to model the bolts in the same reference frame as the rotor, and accept the errors due to the unsteady nature of relative motion between asymmetric features modeled in the same reference frame. The final reference frame setup is summarized in Figure 3.27.
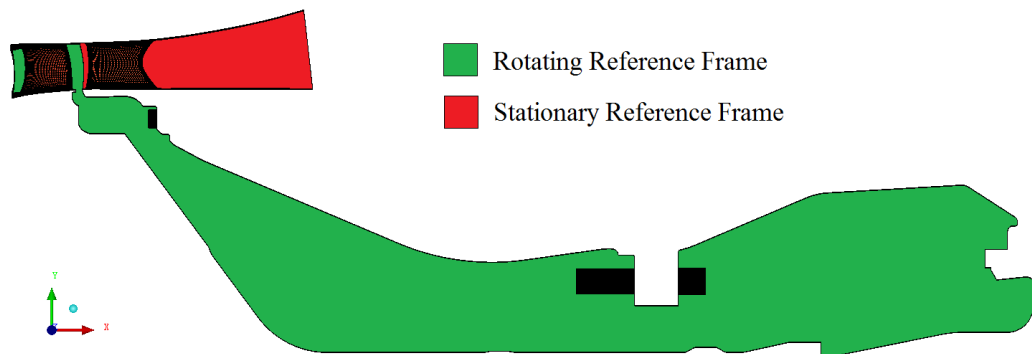

Figure 3.27. Summary of the Reference Frame Setup in the 3D Sector Model

3.5 The 3D CFD model with Merged Gaspath but No Bolts

The final CFD model contains the same merged high fidelity gaspath as the one in Section 3.4. However, the present CFD model does not contain flange bolts or OGV nuts. Although these asymmetric features significantly affect the flow in the cavity, they cause unsteady errors due to modeling them in the same reference frame as the rotor blade. As explained in Section 3.4.2, it proved to be very difficult to place a mixing plane upstream of the nut and bolts due to the swirl in the cavity. Therefore, the next-best option is to run the coupling analysis without bolts and study the effect that including the high-fidelity gaspath has on the analysis.

The Compressor Aero department of Rolls-Royce Inc. previously ran an analysis which solved the flow through the HP compressor for the cycle point of interest. The boundary conditions for the Aero CFD analysis were P_{26} and T_{26} at the compressor inlet, see Figure 3.15. However, the CFD analysis does not always predict P_{30} and T_{30} at the diffuser exit which is predicted by the performance models. The performance models are calibrated by test data and are considered to be more reliable than even a CFD analysis of the type run by Aero. For the coupled analysis in the present Section, pressure and temperature profiles obtained from the previously run Aero analysis were linearly scaled to match performance predictions. This is done by the following equations:

$$P_{scaled} = P_{26,cycle} + \left(\frac{P_{unscaled,CFD} - P_{26,CFD}}{P_{30,cycle} - P_{26,cycle}} \right) (P_{30,cycle} - P_{26,cycle}) \qquad (3.19)$$

$$T_{scaled} = T_{26,cycle} + \left(\frac{T_{unscaled,CFD} - T_{26,CFD}}{T_{30,cycle} - T_{26,cycle}} \right) (T_{30,cycle} - T_{26,cycle}) \qquad (3.20)$$

where $P_{unscaled,CFD}$ and $T_{unscaled,CFD}$ are the unscaled pressure and temperature profiles predicted by the Aero CFD analysis, $P_{XX,cycle}$ and $T_{XX,cycle}$ are the pressures and temperatures predicted by the performance models at the compressor inlet and outlet, and $P_{XX,CFD}$ and $T_{XX,CFD}$ are the pressures and temperatures predicted by the Aero CFD model at the compressor inlet and outlet.

3.6   The Solid Thermal Finite Element Model

The finite element model consisted of 35338 nodes and 14749 six-noded triangular elements. It is not known if any sensitivity study was performed on the model, but the mesh was refined in appropriate regions to minimize spatial temperature errors. The finite element mesh is shown in Figure 3.28.
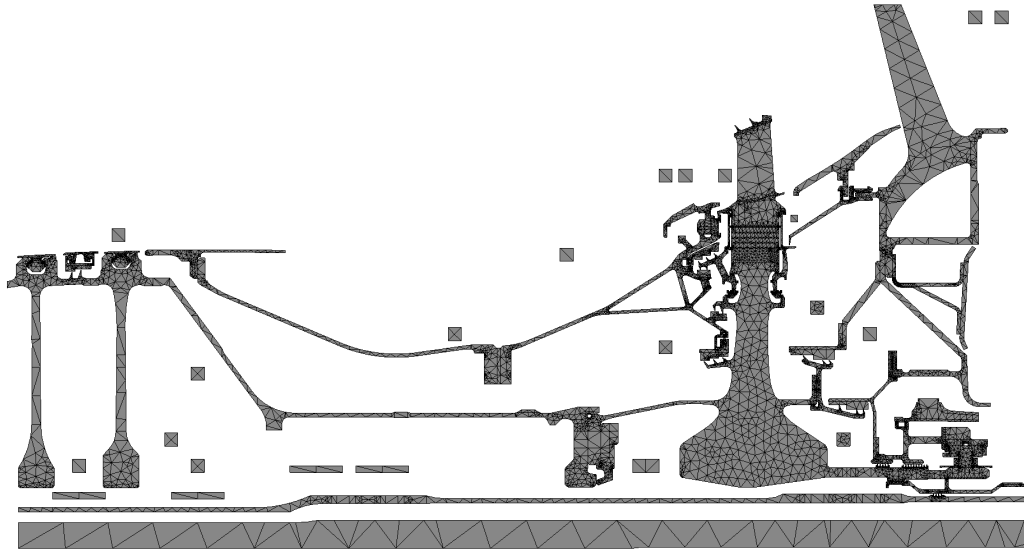
Figure 3.28.   Solid Model Mesh

The boundary conditions for the solid model are summarized in Figure 3.29. The solid model and boundary conditions were setup by the thermals department of Rolls-Royce Inc. [20]. All of the conventional boundary conditions, e.g. streams, ducts, and voids, were previously applied and matched to test data from a previous analysis. The boundary conditions surrounding the cavity walls are given by convecting zone condition which couples the finite element model with the CFD analysis, see Section 2.7.2.
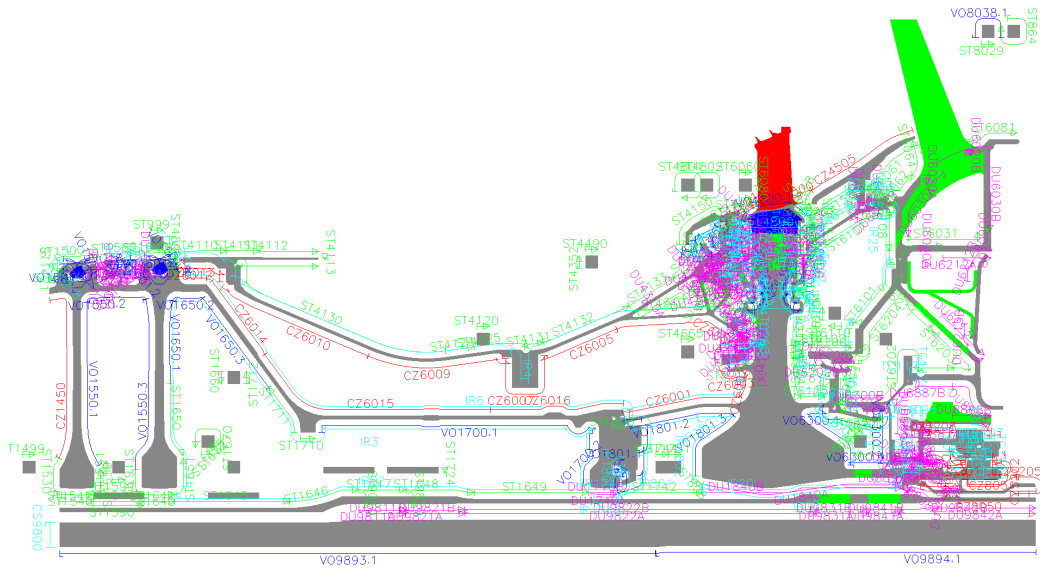
Figure 3.29. Boundary Conditions for Solid Finite Element Model

4. RESULTS

In this chapter the CFD and finite element results will be presented along with comparison to experimental thermocouple data.

4.1 Summary of 5 CFD Models to be Discussed

Five CFD models are compared in this Section:

1. 2D - no bolts, shown in Figure 3.2, is a 2D CFD model that contains an abbreviated gaspath with the inlet temperature matched to thermocouple data. No attempt was made to model the cavity bolts for this model, see Section 3.1.

2. 3D - no bolts, shown in Figure 3.11, is a 3D sector CFD model that contains an abbreviated gaspath with the inlet temperature matched to thermocouple data. No attempt was made to model the cavity bolts for this model, see Section 3.2

3. 2D - with bolts (porous media), shown in Figure 3.12, is a 2D CFD model that contains an abbreviated gaspath with the inlet temperature matched to thermocouple data. The cavity bolts were modeled by using porous media in the bolt regions, see Section 3.3.

4. 3D - with bolts and high fidelity gaspath, shown in Figure 3.22, is a 3D sector model that contains a high fidelity gaspath with the inlet temperature derived from an Aero CFD analysis and performance predictions. The bolts were modeled in 3D, see Section 3.4.

5. 3D - high fidelity gaspath but no bolts, also shown in Figure 3.22, is a 3D sector model that contains a high fidelity gaspath with the inlet temperature derived from an Aero CFD analysis and performance predictions. No attempt was made to model the cavity bolts, see Section 3.5

Cases 4 and 5 satisfy the objective of the thesis because they use predictive boundary conditions derived from computational models. The first three cases use boundary conditions that have been matched to test data and therefore do not satisfy the thesis objectives. All analyses have reached the stabilized max takeoff condition, which means all boundary wall temperatures are equal to to those in the coupled solid finite element model. Various flow fields are compared including total temperature, absolute pressure, swirl fraction, axial velocity, and streamlines. In addition, windage and mass average swirl fraction as a function of axial coordinate are also compared for all five cases.

4.1.1   Normalized Temperature Comparison

The normalized temperature comparison is shown in Figure 4.1.1. The 3D No-Bolt case, Figure 4.1(c), is very similar to the 2D no-bolt case in Figure 4.1(b) which is expected because the 3D case is simply the 2D case swept into a sector. Normalized temperature T* is given as:

$$T^* = \frac{T - T_{26}}{T_{30} - T_{26}} \tag{4.1}$$

The following Figures compare normalized temperature, equation (4.1), between the high fidelity 3D bolt case, Figure 4.1(e), and the 2D porous bolt case, Figure 4.1(d). The cavity inlet temperature for the 3D bolt case are significantly hotter than the porous media bolt case. Then the temperature suddenly cools to temperatures similar to the porous bolt case. This sudden temperature change occurs at the OGV nut, which suggests that there may be flow errors near this nut due to modeling a stationary 3D feature in a rotating reference frame. The 3D case with a high fidelity gaspath but no bolts, Figure 4.1(f), has a hotter inlet temperature than most of the other cases. This appears to show that the Aero CFD model slightly over-predicts the inlet temperature for the drive cone cavity.

66

(b) 2D No-Bolts

(c) 3D No-Bolts

(d) 2D Porous-Bolts

(e) 3D Bolts

(f) 3D No-Bolts HiFi Flowpath
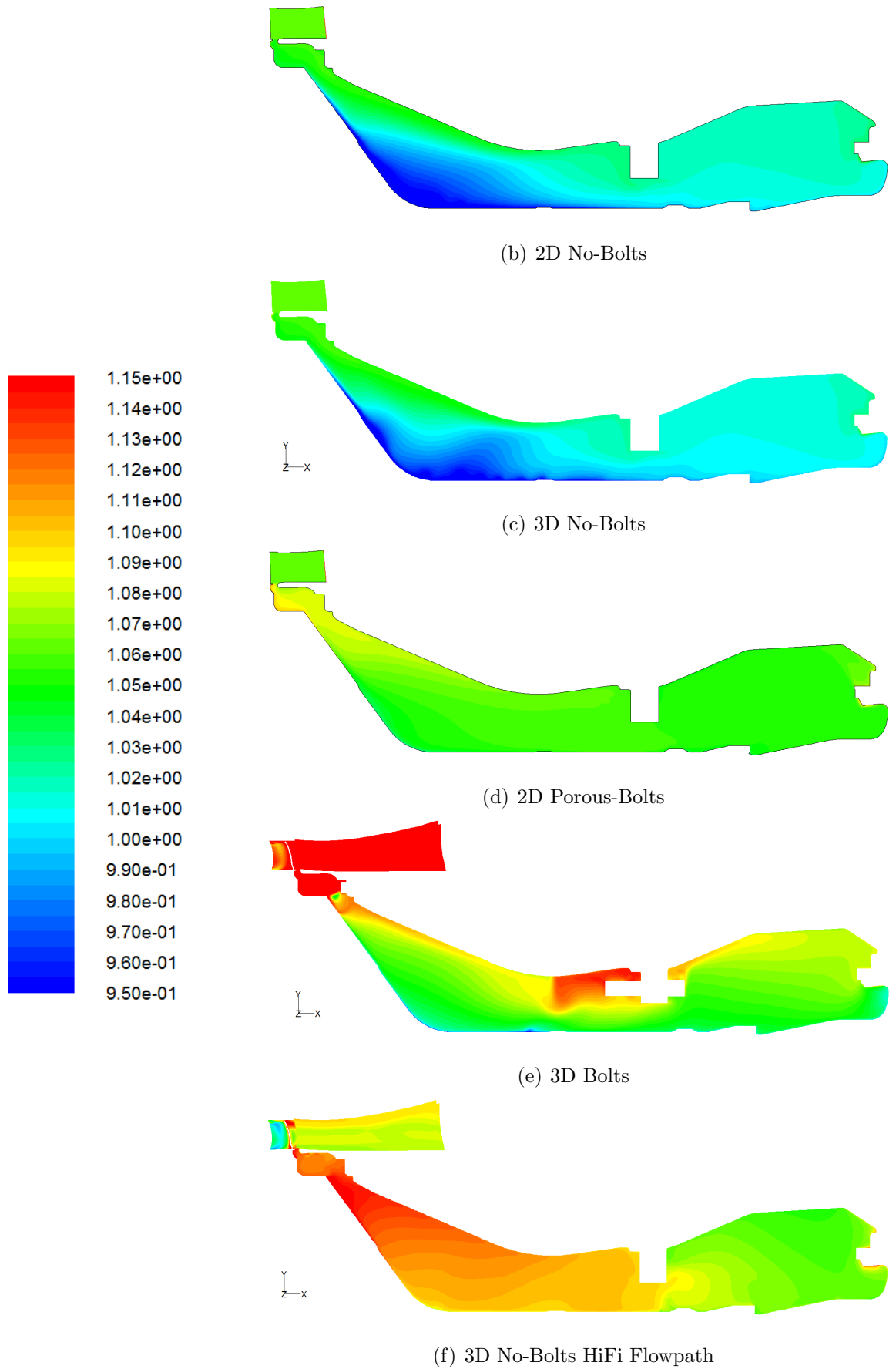
Figure 4.1. Normalized Total Temperature Comparison

4.1.2 Swirl Fraction Comparison

The swirl fraction comparison, given by equation (3.3), is shown in the Figures below. The 3D No-Bolt case, Figure 4.2(c), is very similar to the 2D no-bolt case in Figure 4.2(b) which is expected because the 3D case is simply the 2D case swept into a sector.

The swirl fraction throughout the 3D bolt case's cavity, Figure 4.2(e), is significantly higher than the porous media bolt case, Figure 4.2(d), and both of the no-bolt cases. This does not make physical sense because the 3D bolts should be slowing the tangential velocity of air down to approximately that of the porous-bolt case. This is more evidence that modeling stationary 3D features in a rotating reference frame causes significant flow errors. The swirl fraction in the porous-bolt case is lower than that of the no-bolt cases which is expected. The swirl for the 3D no-bolt case with merged gaspath, Figure 4.2(f), is lower than expected which could be caused by the non-axisymetric effects of modeling a high-fidelity gaspath.

(b) 2D No-Bolts

(c) 3D No-Bolts

(d) 2D Porous-Bolts

(e) 3D Bolts

(f) 3D No-Bolts HiFi Flowpath
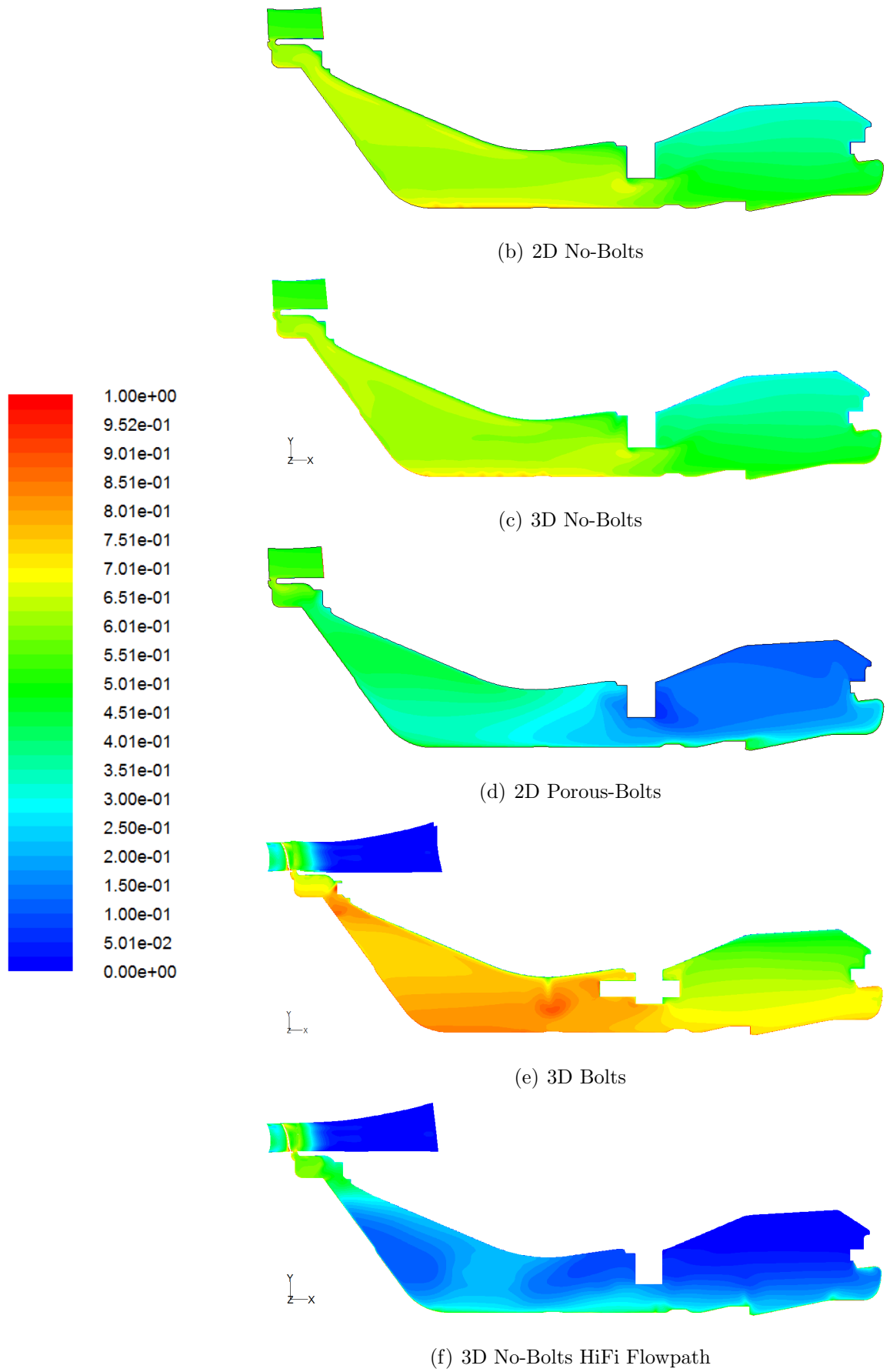
Figure 4.2. Swirl Fraction Comparison

4.1.3   Normalized Pressure Comparison

The normalized pressure comparison is shown in the Figures below. The 3D No-Bolt case, Figure 4.3(c), is very similar to the 2D no-bolt case in Figure 4.3(b) which is expected because the 3D case is simply the 2D case swept into a sector. Normalized Pressure P* is given as:

$$P^* = \frac{P - P_{26}}{P_{30} - P_{26}} \qquad (4.2)$$

The pressure in the 3D-bolts cavity, Figure 4.3(e), is higher than the pressure in any of the other cases. This is likely because the pressure boundary conditions were directly applied from the Compressor Aero without scaling them by the performance cycle predictions. The pressure in the porous-bolts case, Figure 4.3(d), is slightly higher than the pressure in the no-bolt cases most likely because of the resistance to tangential velocity caused by the bolts. The inlet pressure in the 3D no-bolts, high fidelity gaspath model, Figure 4.3(f), is higher than any of the matched inlet boundary condition models, but the pressure throughout the cavity is comparable to the porous bolt case.

(b) 2D No-Bolts

(c) 3D No-Bolts

(d) 2D Porous-Bolts

(e) 3D Bolts

(f) 3D No-Bolts HiFi Flowpath
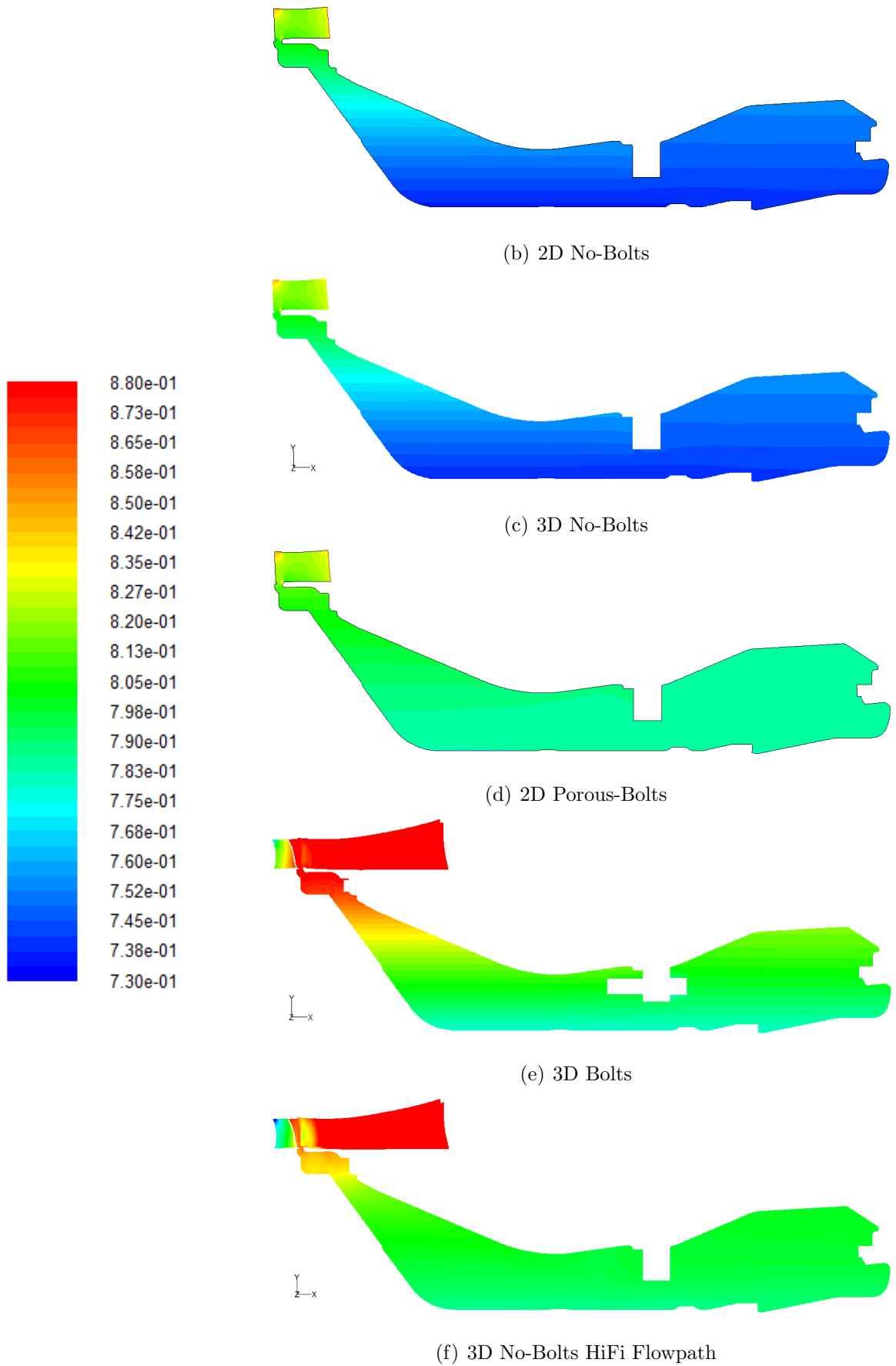
Figure 4.3. Normalized Pressure Comparison

4.1.4   Axial Velocity

As expected, the axial velocity patterns for the 2D no-bolts case, Figure 4.4(b), and the 3D no-bolts case, Figure 4.4(c), are very similar. Axial velocity is normalized by simply dividing it by the axial velocity at the cavity outlet, $V_{ax,out}$ in Figure 3.8. The differences between the remaining 3 cases: the 3D bolt case, Figure 4.4(e); the 2D porous bolts case, Figure 4.4(d); and the 3D no-bolt case with merged gaspath, Figure 4.4(f), are subtle.

(b) 2D No-Bolts

(c) 3D No-Bolts

(d) 2D Porous-Bolts

(e) 3D Bolts

(f) 3D No-Bolts HiFi Gaspath
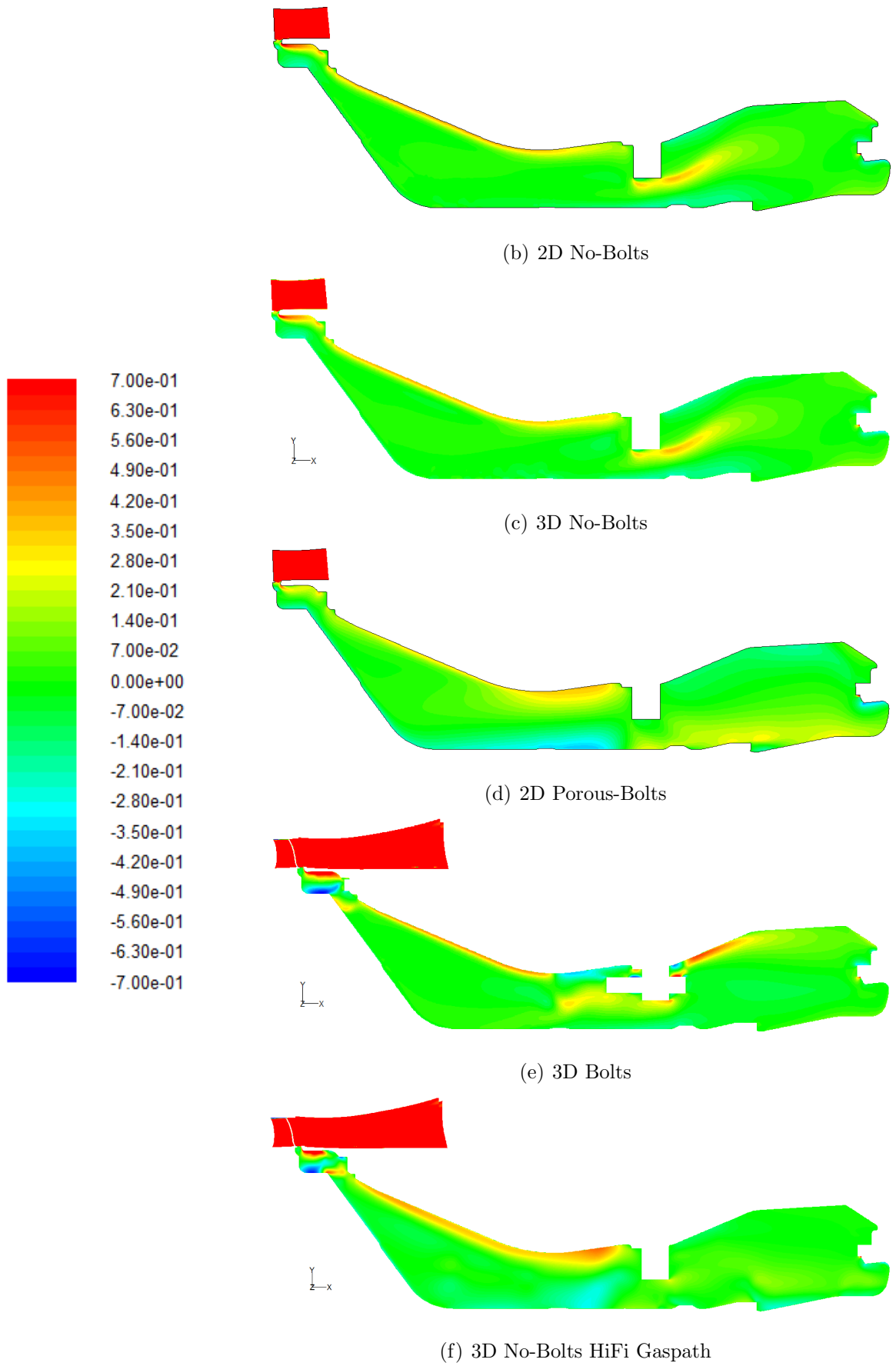
Figure 4.4. Normalized Axial Velocity Comparison

4.1.5   Flow Patterns

The cavity flow patterns are shown by normalized stream function for the 2D cases and by pathlines for the 3D cases. The stream function contour lines for th 2D no-bolt case are shown in Figure 4.5(b), and the 2D porous-bolt case in, Figure 4.5(d). From these diagrams it is clear that the addition of porous bolts induces a significantly different flow pattern in the cavity. The pathlines for the 3D no-bolt case, Figure 4.5(c), show that it has a similar flow pattern to the 2D no-bolt case as expected. The flow pattern from the 3D no-bolt with merged gaspath, Figure 4.5(f), has a similar flow pattern to the 2D porous bolt case which is somewhat unexpected but is likely caused by the addition of the high fidelity gaspath.

(b) 2D No-Bolts

(c) 3D No-Bolts

(d) 2D Porous-Bolts

(e) 3D Bolts

(f) 3D No-Bolts HiFi Gaspath

Figure 4.5. Comparison of Flow Streamlines Colored Using Normal-
ized Axial Velocity Magnitude

4.1.6   Windage Comparison

Windage is a measure of the amount of work a rotating wall puts into the fluid. It can also be considered a measure of the "viscous heating" or "frictional heating" that a wall adds to the fluid. Windage is given by the equation:
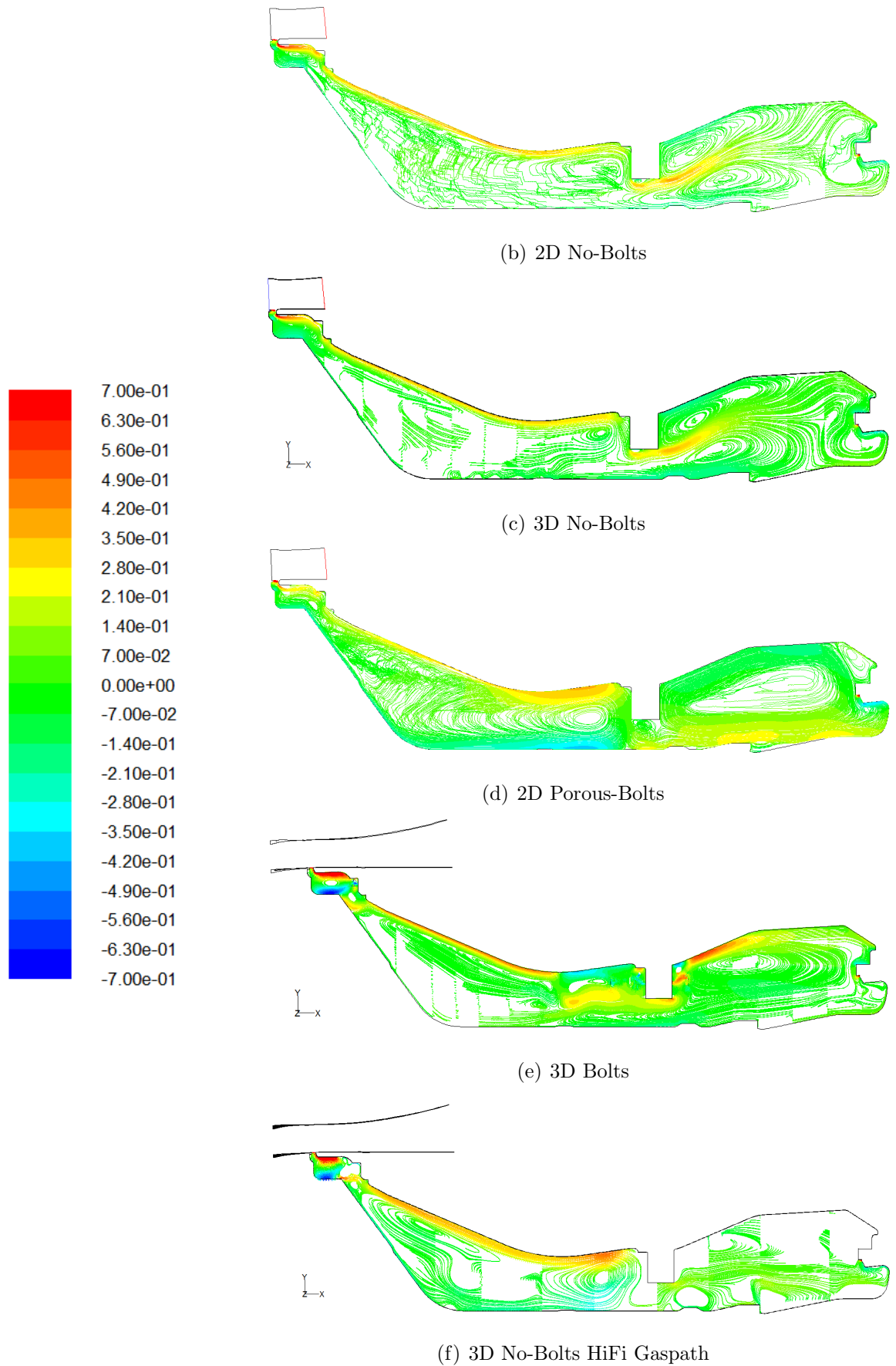
$$W = T_q \Omega = -\tau_\theta r \Omega \qquad (4.3)$$

The windage heating summary in Figure 4.6 shows that the windage heating of the
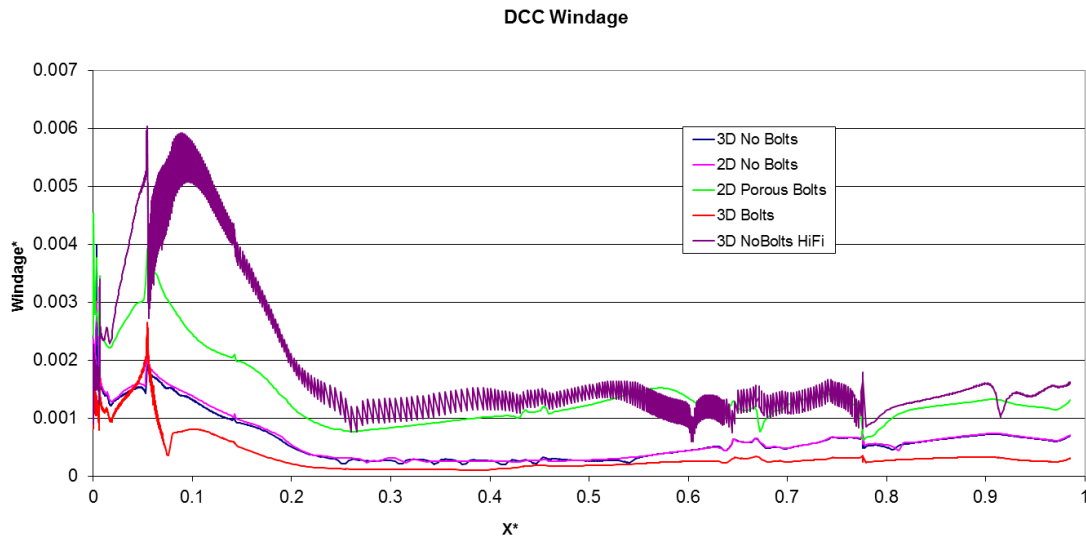
Figure 4.6.   Drive Cone Windage Heating Summary

2D no-bolt case is approximately equal to the 3D no-bolt case, as one would expect. The windage from the 2D porous-bolts case is higher than both of the no-bolt cases which is also expected because the drag from the bolts means that the rotor must do more work to keep the shaft rotating at the same speed. The windage from the 3D bolts case is lower than all of the other cases which is not expected and suggests an error in the analysis. The error is most likely due to the fact that the stationary bolts and rotating rotor blade were modeled in the same reference frame. Relative motion between moving discrete 3D objects causes unsteadiness in the flow. The windage for the 3D no-bolt, high fidelity gaspath case is spread over a band which implies that

the windage is not axisymetric for this case. This is likely the result of the pressure wake off of the rotor blade. On average, the windage is higher than expected for this case because it is higher than both of the other no-bolt cases.

4.1.7   Mass Averaged Swirl Fraction Comparison

The mass-weighted average of swirl fraction was taken across several axial planes spaced through the drive cone cavity for each CFD case that was run. Swirl fraction is a non-dimensional measurement of circumferential velocity, given by the equation:

$$swirl = \frac{V_\theta}{r\Omega} \tag{4.4}$$

where:

V_θ =fluid velocity the circumferential direction

Ω = angular velocity of the engine shaft

r =radial distance to fluid particle
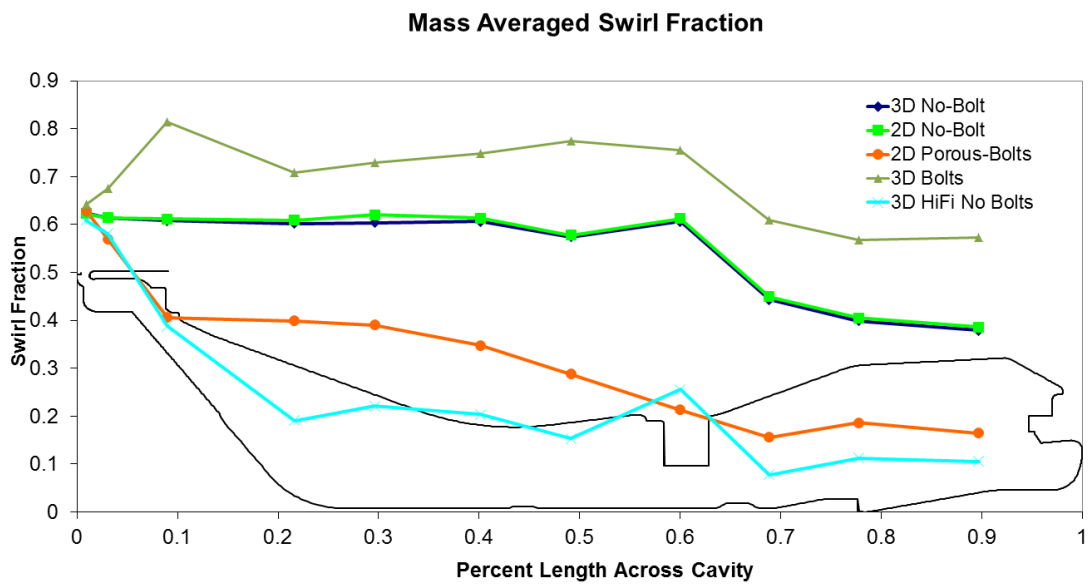
Figure 4.7. Mass Averaged Swirl Fraction Summary

4.2   Metal Temperature Results

In this Section stabilized max takeoff metal temperatures are presented and compared to experimental data. Normalized temperature T* is given by equation (4.1). Normalized metal temperatures for 2D no-bolt case are shown in Figure 4.8(b), and the 3D no-bolt case in Figure 4.8(c). The metal temperatures in the two Figures below are very comparable which is to be expected because the only difference between the two analyses is that the 3D no-bolt CFD case is simply the 2D no-bolt CFD case swept into a sector. These metal temperature results confirm that SC03 is just as capable at coupling a finite element model to a 2D CFD model as to a 3D sector CFD model.

Normalized metal temperatures for 3D bolt case are shown in Figure 4.8(e), and the 2D porous bolt case in Figure 4.8(d). Both of these with-bolt cases have hotter metal temperatures on the cavity walls than the no-bolt cases. For the porous-bolt case this is because the drag due to the porous media bolts required the rotor surface to put more work into the cavity air.

(b) 2D No-Bolts

(c) 3D No-Bolts

(d) 2D Porous-Bolts

(e) 3D Bolts

(f) 3D No-Bolts HiFi Flowpath
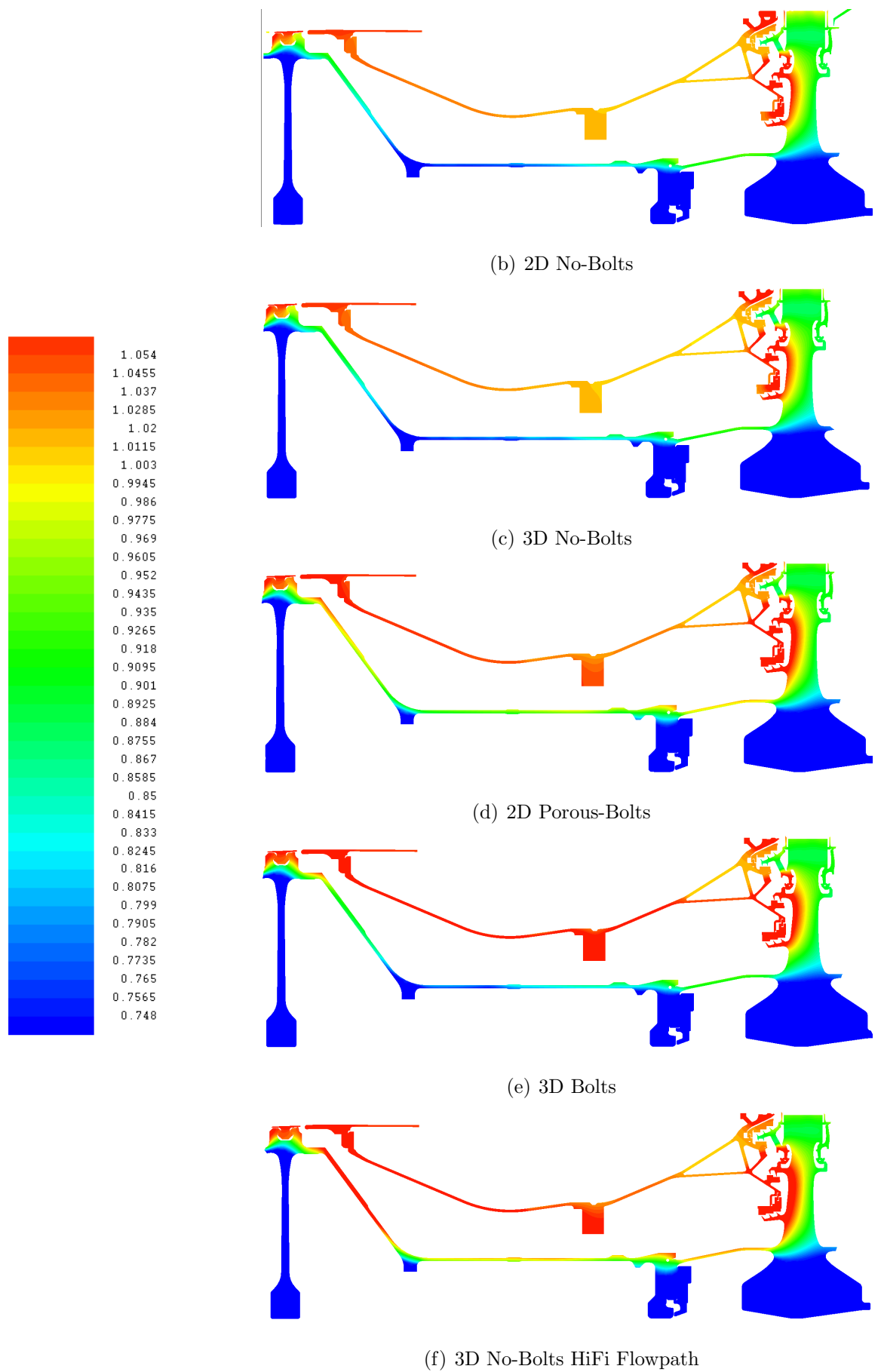
Figure 4.8. Normalized Metal Temperatures

Temperature readings from thermocouples in a test engine are the only available metric for validating the coupled analyses using any given CFD model. Windage generated by the rotor surface is not able to be experimentally measured because the torque on the rotor surface is much less than the torque on the overall shaft. Table 4.1, summarizes the temperature difference, ΔT, between stabilized max takeoff metal temperature results of the coupled analyses and thermocouple test data at specific reference locations.

$$\Delta T = predicted\, metal\, temperature - thermocouple\, temperature \qquad (4.5)$$

Table 4.1. Analysis Comparison to Thermocouple Data. See Figure
4.9 for Thermocouple Locations in the Cavity

| Case	1	2	3	4	5
Inlet BC	Matched	Matched	Matched	Predicted	Predicted
Run Description	2D-No Bolts (K)	3D-No Bolts (K)	2D-Porous Bolts (K)	3D-Bolts (K)	3D-HiFi No-Bolts(K)
Thermocouple					
M5462	-11	-12	-1	13	3
M5463	-14	-14	-7	7	-6
M5465	-9	-9	-3	4	-5
M5467	-6	-7	7	5	13
M5468	-15	-15	-1	-2	2
MH1DFH	-24	-25	-4	-28	4
MH1DFA	-9	-9	13	-10	16
MH6WRW	-23	-23	0	7	7
MH6WARA	-24	-25	9	11	19
MH6WBRA	-32	-31	7	-20	45
MH6WDRA	-35	-33	9	-19	51
MH6WFRA	-49	-49	-1	-47	22
MH6WRRA	-43	-44	4	-37	7
T4389	-1	0	5	41	16
Avg Abs Error	23	23	5	17	17
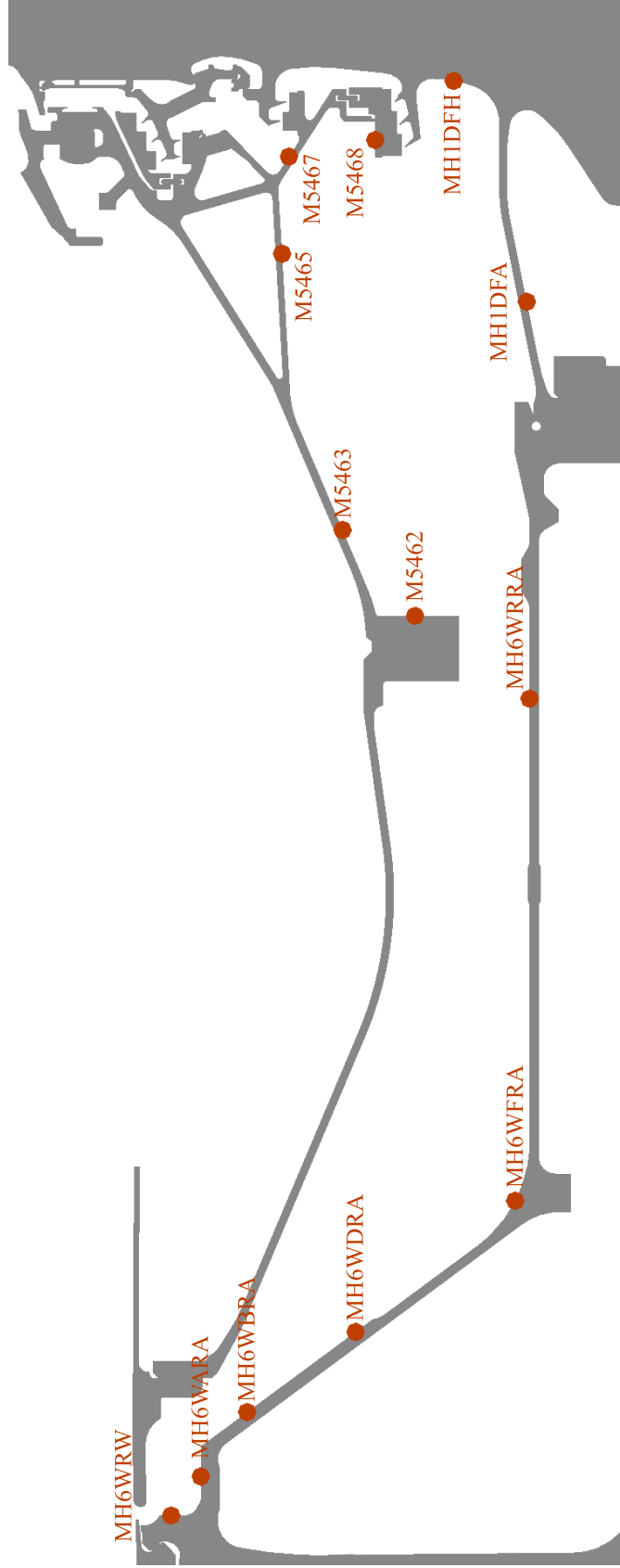
Figure 4.9.   Thermocouple locations in the HP Cavity

5. CONCLUSIONS AND FUTURE WORK

5.1   Conclusions

All four objectives stated in the introduction have been met.

1. The DCC was modeled with a more physically representative inlet condition while coupling the solid thermal analysis and compressible air flow analysis that includes the fluid velocity, pressure, and temperature fields. A portion of the main annulus that includes the HP6 rotor and OGV, figure 1.2, was attached to the cavity inlet, and 3D flange bolts and OGV nuts were added to the CFD mesh.

2. A coupled analysis was run whose boundary conditions come only from computational models, rather than thermocouple data. The performance group of Rolls-Royce predicts the pressures and temperatures on both ends of the high pressure compressor (P_{26} and T_{26} at the compressor inlet, and P_{30} and T_{30} at the compressor outlet). These predictions are then calibrated using experimental data from a test rig. For a new engine design only these predictions, secondary airflow predictions, and the geometry are available. For two cases, cases 4 and 5 in Table 4.1, the analysis used only these inputs rather than thermocouple data from a previous analysis, to predict metal temperatures in the DCC.

3. The model was then validated using available experimental data by comparing the predicted metal temperatures at reference locations to thermocouple data at those locations.

4. The highest fidelity model which included both the merged portion of the gas-path and the 3D bolts, did not predict metal temperatures well. It is believed that the errors due to having stationary bolts in a rotating reference frame,

prevented the flow solution from being accurately solved. Therefore it is concluded that modeling 3D bolts in a drive cone cavity is not recommended unless a mixing plane can be used to put the cavity domain in the absolute reference frame. However, if the cavity does not contain asymmetric features such as bolts, then the analysis is much more likely to give accurate results.

The similarities in the flow patterns for the 2D no-bolt case (case 1 in Table 4.1 and the 3D no-bolt case, case 2, are expected, as the 3D case is simply the 2D case swept into a sector. The inlet temperatures for both of these CFD models were set to match thermocouple data at the cavity inlet. The coupled predicted temperatures are very similar which verifies that SC89 can couple a 2D finite element model to a 2D CFD model just as well as it can couple a 2D finite element model to a 3D CFD model. For both of these cases the high degree of swirl and the low amount of windage heating contributed to the coupled analysis under-predicting metal temperatures by an average of 23 degrees. This is a direct result of not modeling the drag caused by the flange bolts and OGV nuts.

The 2D porous bolts case, case 3, approximated the drag due to the bolts by modeling the bolt domains as porous. The inlet air temperature was also matched to thermocouple data, however, coupling the FE model with this case predicted the temperatures with much greater accuracy. Modeling the bolts as porous media causes drag which increases the windage heating from the drive cone. This coupled analysis predicted metal temperatures with an average error of 5 degrees.

The 3D bolts case, case 4, has an inlet temperature that is derived from performance models and a compressor Aero CFD analysis of the HP compressor. For the aforementioned reasons, this model did not accurately calculate the flow in the cavity. This coupled analysis predicted metal temperatures with an average error of 17 degrees.

The 3D no-bolts case with a high fidelity gaspath, case 5, had an inlet boundary condition which was derived from predictive, computational models, similar to case 4, rather than matching to thermocouple data. Results show that adding the high

fidelity gaspath caused the analysis to predict metal temperatures slightly better than the matched no-bolt case with an abbreviated gaspath, case 1 and 2. This coupled analysis predicted 3D metal temperatures with an average error of 17 degrees.

Table 4.1 also shows how well each case predicted the air temperature which corresponds to the air thermocouple T4389 whose location is shown in figure 3.10. Of course, the temperature boundary conditions of cases 1, 2, and 3 are set to match this air thermocouple so it is expected that the temperature difference for these cases are close to zero. As the table shows, this is true. The inlet temperature difference between the calculated temperature and thermocouple temperature are -1, 0, and 5 degrees for cases 1, 2, and 3 respectively. For the cases whose boundary conditions came from predictive, computational models, the 3D bolts case over predicted the inlet temperature by 41 degrees, and the 3D no-bolt case over predicted the inlet temperature by 16 degrees. Therefore, for the no-bolt case, the predictive boundary conditions performed encouragingly well, though not perfectly.

5.2 Future Work

Future analysis could include modifying case 5 by modeling the bolts in 3D using porous media. A comparison of this model to case 3 would be a direct test of the effectiveness of adding a gaspath and using predictive boundary conditions. Another possible analysis would be to place a mixing plane upstream of the cavity inlet so that the bolts could be modeled in the absolute reference frame. This would be accomplished by pushing the mixing plane back toward the HP6 rotor blade, and adding an additional OGV domain downstream of the mixing plane. The cavity outlet patch would then be moved to the OGV domains rather than the HP6 rotor domain. The cavity mesh could then be merged to the cavity outlet patch of the double-wide OGV domain. Thus the flow around the bolts would be modeled correctly, and their effect on windage and swirl in the cavity would be better captured. For both of these cases, greater time could be taken to ensure that the near-wall mesh refinement

yielded y^+'s in the correct range. Because every mesh refinement required the cavity mesh to be merged to the HP6 rotor mesh node-by-node, this iterative process proved to be very time consuming, and the final results were not perfect. The analysis could be further improved by performing a turbulence model sensitivity study, to see if other turbulence models may be better suited for this type of analysis and/or perform faster. In addition, a 3D bolt CFD analysis could be coupled with a 3D finite element analysis to determine the non-axisymetric temperature distribution of the metal. For all of the coupled analyses presented in this thesis, the goal was to find the steady state max takeoff temperatures in the DCC. This study could be further expanded by finding the transient response of metal temperatures, and comparing the predictions to available experimental transient data. Finally, the CFD analysis itself could be a transient one. Thus, at every time point in the analysis, the transient solid finite element analysis would be coupled to a transient CFD analysis. This would be achieved through a sliding mesh, in which the HP6 rotor would physically move with respect to the cavity mesh. This would be the most accurate (and also the most computationally expensive) way to model the flow off the rotor and around the bolts.

LIST OF REFERENCES

LIST OF REFERENCES

[1] J.M. Owens and R.H. Rogers. *Flow and Heat Transfer in Rotating-Disc Systems.* Research Studies Press Ltd, 1989.

[2] R.D. Monico and J.W. Chew. Modelling thermal behaviour of turbomachinary disc and casings. *Heat Transfer and Cooling in Gas Turbines*, October 1992.

[3] L.V. Lewis and J.I. Provins. A non-coupled cfd-fe procedure to evaluate windage and heat transfer in rotor-stator cavities. *ASME Turbo Expo*, 3, June 2004. ASME Paper GT2004-53246.

[4] J. Evans, L.M. Stevens, C. Bodily, and M.B. Kang. Prediction of velocities and heat transfer coefficients in a rotor-stator cavity. *ASME Turbo Expo*, June 2004. ASME Paper GT2004-53639.

[5] L.A. Verdicchio, C.A. Long, A.B. Turner, G. Kais, and K.M. Tham. Measurement and cfd prediction of the flow within an hp compressor drive cone. *Journal of Turbomachinery*, 125, January 2003. ASME.

[6] J.A. Dixon, J.A. Verdicchio, D. Benito, A.Karl, and K.M. Tham. Recent developments in gas turbine component temperature prediction methods, using computational fluid dynamics and optimization tools, in conjunction with more conventional finite element analysis techniques. *Proceedings of the Institution of Mechanical Engineers, Part A: J. Power Energy*, pages 241–255, 2004.

[7] J.A. Dixon. Gas turbine critical component temperature predictions for fatigue life and integrity considerations. *International Society for Air Breathing Engines and American Institute of Aeronautics and Astronautics*, 1999.

[8] L.V. Lewis and J.A. Verdicchio. Fluent analysis of wall heat temperatures and heat transfer coefficients on a high rotational speed drive cone in an aero-engine high pressure compressor including validation against engine thermocouple measurements. *FLUENT 1996 European Users' Group Meeting*, 1996.

[9] J.A. Verdicchio. *The Validation and Coupling of Computational Fluid Dynamics and Finite Element Codes for Solving Industrial Problems.* PhD thesis, University of Sussex, England, 2001.

[10] A.V. Mirzamoghadam and Z. Xiao. A non-coupled cfd-fe procedure to evaluate windage and heat transfer in rotor-stator cavities. *Journal of Engineering for Gas Turbines and Power*, 124, June 2002. ASME.

[11] C.J. Barnes, Z. Sun, J.W. Chew, N.J. Hills, and K.N. Volkov. Efficient finite element analysis/computational fluid dynamics thermal coupling for engineering applications. *Journal of Turbomachinery*, 132, July 2010. ASME.

[12] L. Lewis, C. Mabilat, Z. Sun, J.W. Chew, and N.J. Hills. Coupled aerothermo-mechanical simulation for a turbine disk through a full transient cycle. *Journal of Turbomachinery*, 134, January 2012. ASME.

[13] J.B. Illingworth, N.J. Hills, and C.J. Barnes. 3d fluid-solid heat transfer coupling of an aero engine pre-swirl system. *ASME Turbo Expo*, 3, June 2005. ASME Paper GT2005-68939.

[14] J.A. Dixon, A.G. Valencia, and A. Bauknecht. Heat transfer in turbine hub cavities adjacent to the main gas path. *Journal of Turbomachinery*, 135, March 2013. ASME.

[15] C.J. Barnes, D. Amirante, and N.J. Hills. Thermo-mechanical finite element analysis/computational fluid dynamics coupling of an interstage seal cavity using torsional spring analogy. *Journal of Turbomachinery*, 134, September 2012. ASME.

[16] U. Javiya, N.J. Hills, J. Chew, and V. Ganine. Coupled fluid-structure transient thermal analysis of a gas turbine internal air system with multiple cavities. *Journal of Engineering for Gas turbines and Power*, 134, October 2012. ASME.

[17] Fluent 6.3. *User's Guide.* ©Fluent Inc., 9 2006.

[18] Fluent 13. *User's Guide.* ©Fluent Inc., 9 2012.

[19] B. E. Launder and D. B. Spalding. *The Numerical Computation of Turbulent Flows*, volume 3. 1974.

[20] C. J. Barnes. Dns163600: Hp turbine disc-coupled analysis of the hp6 drive cone cavity and comparison to thermocouple data. *Internal Rolls-Royce Technical Document*, 11 2010.

[21] M. Mills. Dns153985: Hp6 drive cone cavity cfd: 2d representation of bolts using porous media. *Internal Rolls-Royce Technical Document*, 15 2009.

APPENDIX

SCRIPTS

Script to extract the points where the pathlines cross the HP6 rotor inlet plane. The test value has been removed.

```bash
#!/bin/bash

FILENAME=$1
PREVLINE=""
TESTVAL="X.XXXXX"

while read LINE
do
    if [[ "$LINE" != *.* ]]
    then
        if [[ $(echo "$PREVLINE" | cut -d" " -f1) < "$TESTVAL" ]]
        then
            echo "$PREVLINE" >> process.txt
        fi
    fi
    PREVLINE="$LINE"

done < $FILENAME
```